University of Alberta

Investigating The Potential of Self Assembled Monolayers for Nanosensors

by

Kanwarjit Singh Gill

A thesis submitted to the Faculty of Graduate Studies and Research in partial fulfillment of the requirements for the degree of **Master of Science**.

Department of Electrical and Computer Engineering

Edmonton, Alberta

Fall 2004

Library and Archives Canada

Published Heritage Branch

395 Wellington Street
Ottawa ON K1A 0N4
Canada

Bibliothèque et Archives Canada

Direction du Patrimoine de l'édition

395, rue Wellington
Ottawa ON K1A 0N4
Canada

Your file Votre référence
ISBN: 0-612-95754-3
Our file Notre référence
ISBN: 0-612-95754-3

The author has granted a non-exclusive license allowing the Library and Archives Canada to reproduce, loan, distribute or sell copies of this thesis in microform, paper or electronic formats.

L'auteur a accordé une licence non exclusive permettant à la Bibliothèque et Archives Canada de reproduire, prêter, distribuer ou vendre des copies de cette thèse sous la forme de microfiche/film, de reproduction sur papier ou sur format électronique.

The author retains ownership of the copyright in this thesis. Neither the thesis nor substantial extracts from it may be printed or otherwise reproduced without the author's permission.

L'auteur conserve la propriété du droit d'auteur qui protège cette thèse. Ni la thèse ni des extraits substantiels de celle-ci ne doivent être imprimés ou aturement reproduits sans son autorisation.

In compliance with the Canadian Privacy Act some supporting forms may have been removed from this thesis.

Conformément à la loi canadienne sur la protection de la vie privée, quelques formulaires secondaires ont été enlevés de cette thèse.

While these forms may be included in the document page count, their removal does not represent any loss of content from the thesis.

Bien que ces formulaires aient inclus dans la pagination, il n'y aura aucun contenu manquant.

Canada

"O foolish mind! Why do you grumble, When you are rewarded according to your own actions? (Guru V. Gauri Rag)

– *Guru Granth Sahib*

To:

My Grandfather Sardar Palla Singh Gill

(1904 - 2003)

&

Grandmother Sardarni Harnam Kaur Gill

Acknowledgements

I would like to express my gratitude to my supervisors Dr. Daniel Kwok and Dr. Steven Dew for giving me this opportunity to complete my thesis. I am indebted to them for their stimulating suggestions, encouragement and financial support. During my association with them I have known them as sympathetic, helpful and always eager to pursue new domains of research. Their unflinching commitment for perfection has left a deep impression on me and I am thankful for what I have learned from them. Furthermore, I owe Dr. Kwok lots of gratitude for showing me this way of research and providing an excellent mentoring which I hope would help me in life not only as a professional but would make me a better human.

I would also like to thank the other members of my MSc committee who spared their precious time to read my thesis and provide me with valuable comments: Dr Chris Backhouse, Dr Don Koval and Dr Walied A. Moussa. I thank you all. Also, I would like to thank Dr Larry Kostuik for providing an access to the combustion lab.

I am indebted to my parents and grandparents, uncles and aunts for instilling in me the importance of education and encouraging me to set higher goals in life. Without their emotional and economical support I would not have achieved this milestone in

my life. I am grateful to my brother Vikram for always standing by me and rendering me the feeling and value of brotherhood. It would be unfair, if I don't mention the name of my sister-in-law who was always helpfull and caring during the brief period of time I came to know her.

I am also grateful to all my colleagues in the Nanoscale technology and engineering laboratory and all the machine shop guys for their valuable suggestions, time and skill. In particular, I would like to thank Kelvin for sparing his time to read my thesis and for our many discussions and his tips. Glen Thomas for his help in setting up my experiment. I would also like to thank Chijoke for his brotherly advice and affection. Maggie was always helpful for sharing her fourier transform infrared knowledge.

I am also thankful to my friends Ranjit Dhillon, Satneev Bhamra, Parminder Grewal, Sukhjit Singh Dhindsa and Gurbir Gill for helping and supporting me during difficult times.

My acknowledgement of gratitude would be incomplete if I forgot to thank the almighty for guiding and inspiring this humble being.

Kanwarjit Singh Gill

Nomenclature

C-18	1-octadecanethiol
COOH	1-mercaptohexadecanoic acid
Θ	Fractional occupancy
P	Partial pressure
b	Langmuir constant
R	Reflectance
$\triangle R$	Change in reflectance
T	Transmittance
I_t	Intensity reflected from the exposed surface
I_O	Intensity reflected from the non exposed surface
A	Absorbance
A°	Angstrom
S	Seconds
h	Hour
W	Watt
p	Component of the light polarized parallel to the plane of the incidence light
s	Component of the light polarized perpendicular to the plane of the incidence light
Ψ	Amplitude ratio of the p and s components of the polarized light.

Δ	Phase shift of the p and s components of the polarized light
R_p	Complex fresnel coefficient
R_s	Complex fresnel coefficient
n	Refractive Index
k	Extinction coefficient
t	Thickness of the film
I	Intensity
A	Analyzer Angle
P	Polarizer Angle
kPa	Kilo Pascal
Hz	Hertz
r	Radius of the drop
c	Concentration
R	Radius of the cylinder
ρ	Apparent density
d	Thickness of the deposit
m	Protein mass
K	Kelvin
C_0	Initial concentration
NIR	Near infrared region
FTIR	Fourier transform infrared
HSA	Human serum albumin

Contents

1 Introduction **1**

1.1 An Introduction to Self Assembled Monolayers (SAM's) 1

1.2 Potential of SAM's as Sensitive Receptors for Adsorption Based Sensors 2

1.2.1 Langmuir Isotherm 3

1.2.2 Adsorption Based Optical Sensor 4

1.2.3 Refractive Index Method VS Optical Absorbance 5

1.2.4 Optical Gas Sensor Based on Adsorption 7

1.3 Potential of SAM's as Platforms for Biological Detection 9

1.3.1 Proteins 11

1.3.2 Structure of Proteins 11

1.3.3 Protein Identification 12

1.3.4 Methods for Protein Identification 12

1.4 Organization of this Thesis 13

2 Background on Self-Assembled Monolayers **14**

2.1 Preparation of Gold Surfaces 16

2.2 Thiols on Au (111) 18

3 Use Of SAM's for Hydrocarbon Gas Sensing 20

3.1 Introduction 20

3.2 Methods and Materials 24

3.2.1 Materials 24

3.2.2 Preparation of SAM's 24

3.2.3 FTIR 25

3.2.4 Ellipsometer 26

3.3 Gas Exposure Setup 29

3.4 Surface Characterization by FTIR and Spectroscopic Ellipsometer . . 30

3.4.1 FTIR Measurements 30

3.4.2 Spectroscopic Ellipsometry 31

3.5 Results and discussions 31

3.5.1 Results from Elliposmetry 31

3.5.2 Results from FTIR 33

3.6 Conclusions 36

4 Spectroscopic Ellipsometry for Characterization and Concentration Measurement of Proteins Immobilized on SAM's. 47

4.1 Introduction 47

4.2 Experimental section 50

4.2.1 Protein Deposition Method 50

4.3 Discussions and Results 51

4.3.1 Interpretation of Ellipsometric Data 51

4.3.2 Relationship between Thickness and Concentration 53

4.3.3 Variation in Intensity with respect to the Change in Concentration 54

4.4 Re-usability 58

4.4.1 Experimental Section 58

4.4.2 Analysis with FTIR 58

4.5 Conclusion 59

5 Summary and Future Direction **73**

5.1 Use Of SAM's for Hydrocarbon Gas Sensing 73

5.2 Spectroscopic Ellipsometry for Characterization and Concentration Measurement of Proteins Immobilized on SAM's. 74

List of Figures

1.1 Schematic representation of a typical self-assembled monolayer adsorbed on a metal or metal-oxide support. 1

1.2 Typical Langmuir adsorption isotherm showing concentration VS fractional occupancy. 4

2.1 Schematic representation of a typical thermal evaporation system used for the preparation of gold substrates. 18

3.1 Schematic representation of a 1-octadecanethiol self-assembled monolayer adsorbed on a gold metal support. 23

3.2 Schematic representation of a 1-mercaptohexadecanoic acid self-assembled monolayer adsorbed on a gold metal support. 23

3.3 Schematic of the ellipsometry setup used for the experiments. 26

3.4 Schematic representation of the gas exposure setup used in this experiment. 30

3.5 Schematic illustration of an alkanethiolate adsorbate that is tilted at 30°(α) from the surface normal and twisted $0^0(\beta)$ around its molecular axis. 33

3.6 Typical FTIR spectra of 1-octadecanethiol monolayer 38

3.7 Typical FTIR spectra of 1-mercaptohexadecanoic acid 39

3.8 Variation in intensity with wavelength for C-18 before and after exposure to propane and methane 40

3.9 Variation in intensity with wavelength for COOH before and after exposure to propane and methane. 41

3.10 FTIR spectra of propane and methane in the gaseous phase (data taken from http://webbook.nist.gov/chemistry). 42

3.11 FTIR spectra of C-18 self-assembled monolayers after being exposed to different concentrations of propane and methane at constant pressure (200 kPa) and temperature (295 K). 43

3.12 FTIR spectra of C-18 self-assembled monolayers after being exposed to 20% propane at different pressures and constant laboratory temperature of 295 K. 44

3.13 FTIR spectra of COOH self-assembled monolayers after being exposed to different concentrations of propane and methane at constant pressure (200 kPa) and temperature (295 K). 45

3.14 FTIR spectra of COOH self-assembled monolayers after being exposed to 20% propane at different pressures and constant temperature of 295 K. 46

4.1 Ellipsometry results showing the reflected intensity in the visible region for different samples of FIB deposited on C-18 and reference C-18 and gold. 61

4.2 Ellipsometry results showing the reflected intensity in the visible region for different samples of HSA deposited on C-18 and reference C-18 and gold. 61

4.3 Ellipsometry results showing the reflected intensity in the NIR region for different samples of FIB deposited on C-18 and reference C-18 and gold. 62

4.4 Ellipsometry results showing the reflected intensity in the NIR region for different samples of FIB deposited on C-18 and reference C-18 and gold. 62

4.5 Comparison of the average intensity Vs wavelength between FIB and HSA in visible region. 63

4.6 Ellipsometry results showing the reflected intensity in the NIR region with respect to the change in the concentration of the HSA protein deposited on C-18 monolayers on Au/Ti/Si substrate for various samples at 4 different nominal concentrations. 64

4.7 Ellipsometry results showing the average change in the reflected intensity in the NIR region with respect to the change in the concentration of the HSA protein deposited on C-18 monolayers on Au/Ti/Si substrate for various samples at 4 different nominal concentrations. 65

4.8 Ellipsometry results showing the reflected intensity in the NIR region with respect to the change in the concentration of the HSA protein deposited on COOH monolayers on Au/Ti/Si substrate for various samples at 4 different nominal concentrations. 66

4.9 Ellipsometry results showing the average change in the reflected intensity in the NIR region with respect to the change in the concentration of the HSA protein deposited on COOH monolayers on Au/Ti/Si substrate for various samples at 4 different nominal concentrations. . . . 67

4.10 Change in $tan\Psi$ with respect to the variation in concentration of the protein deposited on C-18 monolayers on Au/Ti/Si substrate for various samples at 4 different nominal concentrations. 68

4.11 Average change in $\tan\Psi$ with respect to the variation in concentration of the protein deposited on C-18 monolayers on Au/Ti/Si substrate for various samples at 4 different nominal concentrations. 69

4.12 Change in $\tan\Psi$ with respect to the variation in concentration of the protein deposited on COOH monolayers on Au/Ti/Si substrate for various samples at 4 different nominal concentrations. 70

4.13 Average change in tanΨ with respect to the variation in concentration of the protein deposited on COOH monolayers on Au/Ti/Si substrate for various samples at 4 different nominal concentrations. 71

4.14 Comparison of FTIR spectra's collected after treating the protein deposited C-18 and COOH substrate with highly ionic solution of (KCl and NaCl) and a high pH buffer solution. 72

Chapter 1

Introduction

1.1 An Introduction to Self Assembled Monolayers (SAM's)

Self-assembly, in general terminology, can be defined as the spontaneous formation of complex hierarchical structures from pre-designed building blocks, involving multiple energy scales and several degrees of freedom. In nature, self-assembly occurs in the formation of membranes from lipid molecules and living cells.

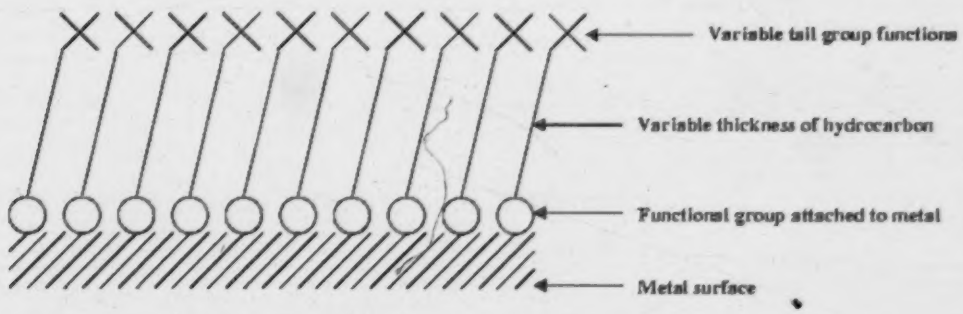

Figure 1.1: Schematic representation of a typical self-assembled monolayer adsorbed on a metal or metal-oxide support.

Self-assembled monolayers as shown in the Fig:1.1 can be defined as the ordered

molecular assemblies that are formed spontaneously by the adsorption of a surfactant with a specific affinity of its head group to a substrate [1]. Various self-assembled monolayer systems are characterized by this head-group-substrate pair. The ordered molecular assembly makes SAM's inherently manufacturable and technologically attractive for building super-lattices and for surface engineering. The stability and the order in these two-dimensional systems are produced by a spontaneous chemical synthesis at the interface, as the system approaches equilibrium [2].

Several systems have been used to form self-assembled monolayers. Since the defining feature for characterizing the monolayer is the pair of the chemisorbing head-group of the molecule and the substrate, the rest of the molecule can literally be quite freely chosen. This property makes SAM's an ideal candidates for surface engineering and it is this property of SAM's that make them attractive for use in surface adsorption-based sensors. Some of the frequently used compounds for making SAM's are extensively covered in the literature [1, 2, 3, 4].

1.2 Potential of SAM's as Sensitive Receptors for Adsorption Based Sensors

Sensors are used in a variety of applications and industries. For example, demand is increasing for small, inexpensive sensors for the detection of hydrocarbon gases for safety, process control and environmental monitoring. According to Sensor Business Digest, the overall North American market for gas sensors/analyzers totaled about $827.3 million in 2001. During the last two decades, the scientific community has witnessed remarkable research activity aimed at the realization of optical sensors for

the measurement and detection of chemicals. It is known that when thin films come into contact with an adsorbent, there is a change in the optical properties of the thin films, and it is this phenomenon which can be exploited for gas sensing. A number of different techniques have been used for gas detection such as: (1) surface plasmon resonance [5], (2) surface acoustic waves [6], (3) micro hotplates [7] and (4) immobilized enzymes [8]. Some of the disadvantages of these sensors are: insufficient sensitivity to hazardous chemical environments, susceptibility to electrical noise, large sensor size, expensive to manufacture, and fire hazard in a flammable environment.

1.2.1 Langmuir Isotherm

All of the sensors developed so far suffer from problems, and the search is still on for a sensor capable of meeting all these requirements. Hope lies in the development of a novel optical gas sensor, based on adsorption phenomena on ultra thin surfaces. Gas adsorption can be modelled by the Langmuir adsorption isotherm [9, 10, 11]:

$$\theta = \frac{bP}{1 + bP} \tag{1.1}$$

where θ is the fractional occupancy (the ratio of number of occupied sites to the total number of sites present), P is the partial pressure of the target gas and b is the Langmuir constant. This constant is a function of temperature, energy of adsorption and the area of the binding site. Since the surface area of a given receptor film is constant, variation in surface energy and temperature is a way to achieve selectivity and sensitivity.

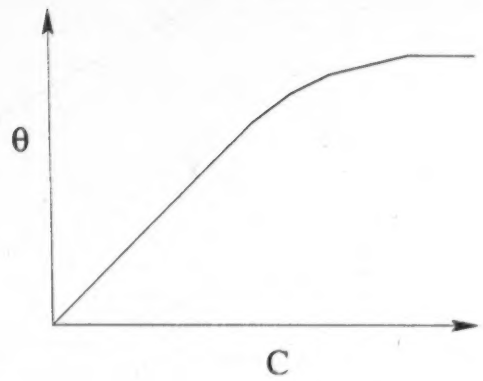

Figure 1.2: Typical Langmuir adsorption isotherm showing concentration VS fractional occupancy.

From the characteristic shape of the Langmuir isotherm shown in Fig.1.2, it is evident that at low concentration the fractional occupancy θ is proportional to the concentration of gas. However, as shown in Fig.1.2 at high concentrations all the binding sites are occupied ($\theta = 1$) and no more gas can be adsorbed [12]. Therefore the response of the sensors based on adsorption is linear only at low concentrations.

1.2.2 Adsorption Based Optical Sensor

It has been shown in the past that the optical properties of a material change with the adsorption of an analyte on a surface. This is a common method used in infrared-spectroscopy and spectrophotometry. Interest is shifting to adsorption based gas sensors that use optical techniques to determine gas composition and concentration to avoid the complications which arise with sensors based on enzymes and other methods.

The general method for optical technique is to have a thin film on a optically non-absorbing substrate. The thin film is composed of molecules with favorable surface

energy for the adsorption of analytes of interest. The adsorption of the gas molecules results in a change in the optical parameters of the thin film. This change in properties can then be used to calculate the concentration of the adsorbed molecules.

In the past adsorption of gas was measured by changes in the thin film's refractive index. This method was based on the concept of multiple beam interference or, to be more precise, on the principle of an anti-reflectance coating [13, 14, 15]. Using the above method, Peterson et al. made Langmuir-Blodgett (LB) films of azo-dyes and polysiloxanes which were deposited on silicon dioxide to measure the concentration of NO_2. It was observed that the use of a LB film as an anti-reflective coating resulted in a change of reflectance (ΔR) after the adsorption of the gas on the thin film. This change was relatively large compared to the reflectance (R) on a control medium, resulting in a high sensitivity. Furthermore, Peterson showed that many factors tend to effect the performance of the NO_2 gas sensor such as the type of substrate, angle of incidence, wavelength of light used, type of materials used. It was also discovered that using materials with high polarisibility [16], and the selection of wavelength [14] has a substantial effect on the reflectance from the surface. Further, it was shown that the choice of material plays an important role in the response time [17].

1.2.3 Refractive Index Method VS Optical Absorbance

Peterson and his co-workers originally used changes in refractive index to relate gas adsorption to changes in optical properties of thin films. It was soon realized that instead of refractive index, optical absorption was much more representative of gas adsorption [18].

Light energy is dissipated after absorption of light within a medium. When the molecules absorb light in the infrared region they often vibrate through bond bending or bond stretching [19]. Absorption of the radiation can be measured by the absorbance or transmittance. Transmittance is defined as,

$$T = \frac{I_t}{I_o} \tag{1.2}$$

where I_t is the energy reflected from the surface which has been exposed to the gas, and I_o is the incident light energy from the surface which has not been exposed to the gas. Absorbance is related to the transmittance by,

$$A = log_{10}\frac{1}{T} \tag{1.3}$$

An increase in fractional occupancy θ results in an increase in the absorbance or a decrease in the transmittance of light from the surface. Peterson constructed a sensor to measure NO_2 gas concentration based on optical absorption. It was observed that the activation energy strongly effects the performance of the gas sensor. The activation energy is the binding energy of the gas molecule to the thin film. Activation energy cannot be decreased randomly, because it has a trade-off with both sensitivity and response time. It was also observed that surface temperature was fundamental for achieving selectivity and reversibility of the surface. Any variation in the temperature of the surface alters the thermodynamic conditions necessary for the gas molecules to desorb or adsorb on the surface.

Past work has shown that gas adsorption is a very fast process [20]. The time constant for adsorption is of the order of 10^{-7} second, although other effects like

boundary layer diffusion may slow down the process. Peterson's sensor was found to have a response time of approximately 10 seconds. Moreover, he found that the time response of the sensor was based on gas molecules diffusing into the film. With further experimental studies it was shown that diffusion was a major factor influencing the response time in Langmuir Blodgett thin films with long molecules. Moreover, these films are not robust and degrade rapidly with time [6].

However, a novel sensor could be developed which is not plagued by these problem. The diffusion problem can be tackled by using ultra thin films, such as self assembled monolayers on a gold substrate. However there are some questions which needed to be answered before using them. Research is needed to determine the wavenumber/wavelength of the light source and the type of the surface best suitable for a particular type of gas.

1.2.4 Optical Gas Sensor Based on Adsorption

Although their are many sensors available in the market based on different physical phenomenons. Their is an opportunity to introduce a novel sensor which is easy to manufacture, inexpensive, sensitive and can be used in the flammable environments. It is possible to make a sensor based on adsorption of gas on ultra-thin films, such as self-assembled monolayers, using optical techniques. However, for a surface to sense optically, it should be thermodynamically inclined towards adsorbing the gas of interest, while not adsorbing any other gases which optically absorb at the same wavelength.

To realize the above goal emphasis has to be laid on the selection of the surface

material. Formation of self-assembled monolayers (SAM's) of alkanethiols on metal surfaces (i.e.nanoparticles) offers a simple and attractive method of surface modification. SAM's can be modified using thiol adsorbates with different ω-terminal functional groups [21, 22, 23, 24]. SAM's have been used in many chemical and biological sensor technologies because of their ability to functionalize a metal surface for specific analyte capture and protect fragile biological molecules from denaturing upon exposure to bare metal surfaces [25, 26, 27].

Though SAM's hold great promise for gas sensing, few efforts have been made in the past. It has been shown in previous studies, that various organic molecules in their vapor-phase adsorb on alkanethiol SAM's [28, 29, 30] depending upon the functional group. It was also observed that the selectivity of the surface depends on the ability of the functional group to accommodate the adsorbate molecule within its structure [31]. Although these results were for organic molecule adsorption on SAM's, the same principle can be applied for gas adsorption. T. Nomura et al. [6] used polymer SAM's as thin films for gas sensing. Polymer SAM's are an excellent material for sensing because they are easy to fabricate and the adsorption phenomenon is reversible. Alkanethiol SAM's may show more promise since they are more closely packed and their ability to change functional groups [2, 1] make them more adaptable for micro-contact printing for easy manufacture of an array of sensors.

There has been some work done in the past to study the adsorption characteristics of different self-organized polymers as sensitive coatings. It was reported [32] that the analytes are best detected when the active surface is composed of highly

symmetrical cavities suitable for the inclusion of analytes. Furthermore, these surfaces can be customized to produce a highly selective and sensitive surface. Several materials were analyzed and it was found that molecules like Calis[N]Arene in a polyurethane matrix have highly symmetric cavities which make them ideal for analyte sensing [32]. Molecules like alkyl-chlorosilanes and trimethylchlorosilane, on quartz substrates, were found to have short response times, good reversibility and excellent sensitivity. Lastly, an alkanethiol monolayer on gold was shown to work as a sensitive surface for discriminating used oil from new oil when it was exposed to the oil in a gas phase [32].

The real difficulty in designing an optical sensor based on adsorption is the selection of the sensitive surfaces for the analytes of interest. In this study, self assembled monolayers of alkanethiols were chosen on the basis of the promise they hold as reported in the past (for more details refer to chapter.2). Building on this promise, different monolayers were examined for hydrocarbon gas detection using FTIR and ellipsometry and the results reported in chapter.3.

1.3 Potential of SAM's as Platforms for Biological Detection

In addition to their utility for gas detection, there is interest in the use of SAM's for a broader array of adsorption sensing. Research is going on to improve the existing and find new sensor technologies capable of biological detection because of the huge demand for medical diagnostics and pathogen detection. Development of large-scale biosensor arrays composed of highly miniaturized signal transducer elements that en-

able real-time and parallel monitoring of multiple species is an important driving force in biosensor research. This is particularly significant in high-throughput screening applications such as drug discovery and proteomics research where many thousands of ligand-receptor or protein-protein interactions must be rapidly examined. In these situations, it is necessary to utilize sensor platforms that have as many of the desirable characteristics of SAM's as possible. The ability to choose functional groups at the end of the chain length gives SAM's the required flexibility to design platforms which are capable of binding targeted proteins.

SAM's of alkanethiols on gold were chosen because they provide practical systems around which the surfaces can be designed and synthesized [33, 34, 35]. Using these systems, it is relatively straightforward to tailor both the physical and chemical properties of biologically relevant interfaces [36]. The ease with which simple alkanethiols can be synthesized and the compatibility of these synthetic methods with biochemical functional groups make it straightforward to present even structurally complex groups at the surface of SAM's [33, 34, 35, 37, 38].

There are several advantages associated with alkanethiols SAM's:(1) they form dense, well ordered, tightly bonded films, (2) they provide a simple motif for selective tailoring of surface chemical properties and, (3) they protect the fragile biological molecules from contamination upon exposure to bare monitoring of metal surfaces [39]. These features are important in many areas of scientific study like chemical and biological sensor technologies [40, 41, 42], molecular electronics [43, 44, 45, 46], lithography [47, 48], and biomimetics [49].

In this study, the main area of thrust is to determine whether ellipsometry can be used for characterizing and measuring the concentration of the proteins. For immobilizing the proteins, we have used SAM's as platforms for their suitability as already explained in the above discussion.

1.3.1 Proteins

What are proteins? Proteins are the fundamental molecules that constitute the human body and carry out the task of life. Proteins are large molecules and their molecular mass can vary from few thousand g-mol^{-1} to more than a million g-mol^{-1} [50]. Proteins were discovered in 1838 by a Swedish chemist called Jons Jacob Berzelius [50] and are recognized as the fundamental ingredients of cells. They represent more than forty percent of the dry mass of the human body. Their has been a lot of emphasis on understanding the proteins but only 3 percent of them have been adequately described so far out of an estimated 30 thousand different proteins. Protein molecules vary in shapes and sizes and they can be anything from compact soluble globules which can pass through cell membranes and initiate metabolic reactions to long insoluble fibres which make up body tissues and hair. In their proper shape, they direct our bodies' activities, channel resources, defend our body against infections and keep us fit whereas, in their mutant form they can cause diseases like cancer or mad-cow.

1.3.2 Structure of Proteins

Proteins at the fundamental level are made up of amino acids whose identity and order are dictated by the genes according to the sequence of DNA bases. Forces

due to chemical bonds between these amino acids like hydrogen bonds, electrostatic interaction between positive and negative charges, and disulfide bridges cause a protein molecule to coil or fold into a secondary structure (i.e. α-helix and β-sheet). Final macroscopic dimensions and tertiary structure of the protein is determined by the forces between these secondary structures. In this study, fibrinogen from human plasma and albumin from human serum were used as the protein samples.

1.3.3 Protein Identification

Protein identification is of paramount interest because of its use in disease detection and identifying bio-chemical hazards. The composition and sequence of the amino acid as well as the molecular weight of the protein produced by certain types of bacteria are different from those of the protein forming the coat of a particular virus [51]. Every microbe produces proteins which are unique for that particular organism and can act as a signature for its identification. Therefore, the ability to identify proteins can aid in diagnosing diseases. Translating the signature proteins into unique optical responses can aid in the early detection of diseases.

1.3.4 Methods for Protein Identification

There are several methods presently used for the identification and measurement of the concentration of proteins like mass spectrometry [52], protein structure-NMR [53], X-ray crystallography [54, 55] and optical techniques. For this experimental study we have placed an emphasis on doing a preliminary investigation to determine the possibility of using spectroscopic ellipsometry as an optical technique for protein

identification and measurement.

Optical techniques are based on the principal that the properties of the light beam change upon reflection, refraction or scattering. Changes in the optical properties of the light after reflection from thin films can be used to determine the changes in the light intensity reflected from the surface, and even the bonding state of the protein layer can be obtained from this. Most of these techniques are based on determining the changes in the amplitude, phase or wavelength of the light used for sample interrogation.

1.4 Organization of this Thesis

This chapter has laid out some of the background and principles of the use of SAM's as the platform or active elements for adsorption -based gas sensors. The next chapter expands on how SAM's are formed, preparation of gold surfaces and the selection of thiol's on Au (111) geometry. Chapter three deals with an experimental study of two prospective SAM's as gas sensors for model hydrocarbon gases. Chapter four deals with characterization of two model proteins and the measurement of protein concentration using ellipsometry respectively. Finally Chapter five provides a summary of conclusions and presents some suggestions for future work.

Chapter 2

Background on Self-Assembled Monolayers

The field of self-assembled monolayers (SAM's) has witnessed tremendous progress in the past decade in terms of synthesis and characterization [56]. In 1946, Zisman published the preparation of a monomolecular layer by adsorption (self-assembly) of a surfactant onto a clean metal surface [57]. His publication did not evoke much interest because the potential of self assembly was not realized at that time. Work initiated in Kuhn's laboratory at Gottingen [1], applying many years of experience in using chlorosilane derivative to hydrophobize glass, was followed by a more recent discovery, when Nuzzo and Allara showed that SAM's of alkanethiols on gold can be prepared by adsorption of di-n-alkyl disulfides from dilute solutions [58].

The success of SAM's based on alkanethiols was mainly due to their advantage over the moisture-sensitive alkyl trichlorosilanes, as well as working with crystalline gold surfaces. Many other self-assembled systems have been investigated, but monolayers of alkanethiolates on gold are the most studied SAM's to date. For a further account on the history of organic thin films refer to [59, 60].

The formation of monolayers by self-assembly of surfactant molecules is one example of the general phenomena of self-assembly. Nature has its own self assembly which results in supramolocular hierarchical organization of interlocking components that provide very complex systems [61]. Self assembly of SAM's offer unique opportunities to increase fundamental understanding of self organization, structure-property relationships, and interfacial phenomena. Interest in SAM's is growing mainly because of the flexibility to tailor both head and tail groups of the constituent molecules which makes them an excellent raw material for many molecule-substrate and molecule-solvent interactions.

SAM structures provide the design flexibility both at the material level and at the molecular levels. This flexibility is necessary to investigate specific interactions involving different substances at a molecular level, and to investigate the effect of increasing molecular complexity on the structure and stability. Research into these phenomena may lead to the actual utilization of SAM's in industrial and medical applications.

There has been tremendous growth in the SAM research particularly in recent years due to the national initiatives taken by various governments around the world in the field of nanotechnology. Nanotechnology from its infancy has moved into interdisciplinary areas and people are engaged in research where physics, chemistry, life sciences and engineering intermingle.

Interest in the general area of self-assembly and specifically in SAM's stems partially from their perceived relevance to science and technology. In contrast to ultrathin

films made by physical and and chemical vapor deposition, SAM's are highly ordered and oriented and can incorporate a wide range of groups both in the alkyl chain and at the chain terminal [2]. A variety of surfaces with specific interactions can be produced with fine chemical control [62]. Their flexibility, dense and stable structure, biocompatibility and biomimetic nature make SAM's an ideal candidate to be used as films for coating to prevent corrosion and applications in biochemical and chemical sensing.

2.1 Preparation of Gold Surfaces

Gold as a substrate is an excellent choice from an experimental standpoint and it is relatively easy to work with. Gold is quite robust in terms of its inertness to oxidation and contamination, unlike copper which oxidizes rapidly upon exposure [3]. For using gold films, a modest setup is required and there is no need to build a cleanroom facility. It is relatively easy to obtain high quality self assembled monolayers on gold surfaces even in an environment which is not clean and where the gold is routinely exposed to different airborne contaminants and organic compounds. The reason for the high quality can be attributed to the thiols and di-sulfides, which displace these weakly adsorbed organic and other airborne materials during the assembly of self assembled monolayers on a gold substrate [3].

For coating silicon and other substrates with gold, evaporation is a commonly used method. In this method heated gold is evaporated onto and condensed onto a relatively flat silicon substrate to produce a thin film (1000 Å). Evaporation of

gold on silicon was accomplished using a resistive thermal source within a vacuum chamber that is capable of reaching pressures of 10^{-6} Torr. Electrical current is passed through a metal resistive heater which is raised to a temperature where the source material evaporates and deposits onto the cooler silicon substrates. Operationally this process is not complex and can produce several gold surfaces of relatively large area ($\geq 100\text{cm}^2$) inexpensively and of extreme purity.

The typical evaporation rate used in these experiments, is approximately 2 Å/S which ensures smooth and atomically flat surfaces. The choice of the resistive heater material depends upon the material to be evaporated on the silicon substrates. Titanium and gold were evaporated using alumina coated tungsten resistive heaters and tungsten resistive heaters respectively.

The reason for coating silicon substrate with titanium before evaporating gold on it has to do with the adhesion of gold onto silicon. The level of adhesion between the deposited gold film and the silicon substrate is very weak and an interlayer of titanium ≥ 100 Å is often used to enhance the adhesion [3].

An important requirement for the evaporation process is that the deposition for both the layers should be carried out without breaking the vacuum. To accomplish this, an evaporation chamber was used with two individually addressable evaporation sources for titanium and gold. As evident in Fig. 2.1, cleaned silicon substrates are placed on a stainless steel slab with their smooth side facing down towards the evaporation source. This is a two step process accomplished by first evaporating titanium onto the silicon substrates and then evaporating gold on the deposited titanium. The

gold in the resistive boat is shielded from the cross contamination of titanium by using a Pyrex glass divider.

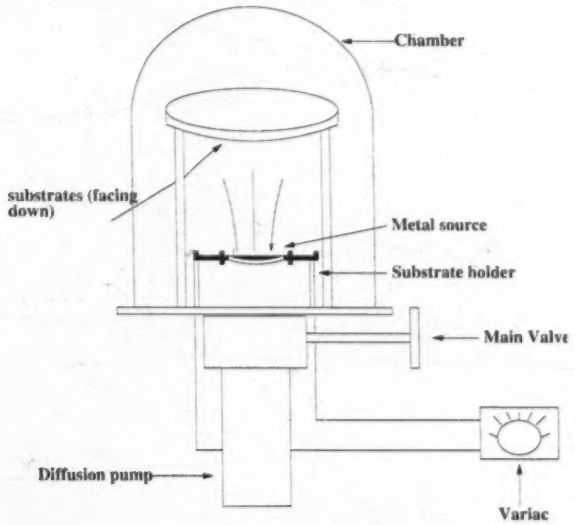

Figure 2.1: Schematic representation of a typical thermal evaporation system used for the preparation of gold substrates.

Gold prepared by evaporation at room temperature is polycrystalline and has a predominately (111) texture [63]. The gold surface made by this process has a rolling hills topology [3] and consists of crystallites of 40 nm × 80 nm with typical peak-to-valley heights of 3 nm between grains [64].

2.2 Thiols on Au (111)

Alkane thiol compounds on Au (111) are the most popular SAM systems. Other popular systems include organo-silicon monolayers on hydroxylated surfaces; however, these typically do not exhibit the degree of long-range order observed for thiols on Au(111) [1, 2, 3, 65]. There are several reasons for the popularity of thiols on Au (111); their ease of preparation [2, 3, 65], well defined order [1, 2, 3, 65] and relative

inertness of the substrate [1, 3, 65]. Another reason for choosing Au (111) topology is the low surface energy. The higher the surface energy, the more chance of absorbing impurities from the atmosphere which would make the SAM sensor less selective. Surface energetics become even more important when the analyte to be sensed is a protein as they are susceptible to contamination.

Considering the relative stability, low surface energy, ease of engineering and suitability to biological samples, it is logical to opt for SAM's of alkanethiols on Au (111) as the system of choice in many research studies.

Chapter 3

Use Of SAM's for Hydrocarbon Gas Sensing

3.1 Introduction

There has been a growing interest in gas sensing in the last decade because of its use in a variety of applications and industries. Demand is increasing for small, inexpensive gas sensors. Different sensing methodologies have been applied in the past depending upon the cost, environment, and the type of the gas to be sensed. Industrial interest in small, inexpensive and sensitive sensing elements for safety and environmental monitoring is one of the driving forces behind the research work for the development of gas detection using thin organic films [66].

Many physical principles have been discovered upon which the sensing systems could be developed. These principles include for example systems based on: resistivity changes, optical changes including surface plasmon resonance and electrochemical phenomena. However, the challenge lies in the production of inexpensive, small, selective, sensitive and easy to manufacture sensors. As an alternative approach, sensors based on optical effects using ultrathin organic films can be of interest for gas

sensing.

Gas adsorption is a very fast process [20]. The time constant for adsorption is of the order of 10^{-7}s seconds. Peterson's [13] sensor had a response time of approximately 10 seconds. He found that the response time of the sensor is based on the gas molecules diffusing into the thin film. Time response can be improved by the use of ultra thin films, for example self assembled monolayers (SAM's) on gold substrates. Sensors based on surface acoustic wave (SAW) devices using SAM's have been tested [67] and they have been found to be better in terms of response time [6] and durability [6] in comparison to sensors designed using Langmuir Blodgett film. Moreover, SAM's can also be used to tailor surfaces which are sensitive to a particular gas and this property can be exploited to make sensor array on a single chip by micro-contact printing to sense different gases. SAM's have also been used in many chemical and biological sensor technologies because of their ability to functionalize a metal nanoparticle for specific analyte capture [25, 26, 27]. Although SAM's hold great promise for sensors based on gas adsorption, few efforts have been made in the past. There are some examples in literature of the vapor-phase adsorption of various organic molecules on alkanethiol SAM's [28, 29, 30]. It was observed in these studies that they adsorb differently on the SAM's depending on the functional group. Furthermore, it was concluded that the selectivity of the surface depended on the ability of the functional group to accommodate the adsorbate molecule within its structure [31]. Although these studies were performed on organic molecules, the same principle could be applied for hydrocarbon gases such as propane, methane and

also hydrogen.

Also, surface energetics play an important role in the adsorption of a gas molecule at the surface of interest. Surfaces with different energies can be realized by varying the chain length of the SAM's or by changing the temperature of the surface. With a change in surface temperature, suitable thermodynamic conditions can be maintained which are essential for the gas molecules to desorb or adsorb at the surface. Furthermore, surface energy is key in designing reusable surfaces. However, for a surface to sense optically, it should be thermodynamically inclined towards adsorbing the gas of interest, but not adsorbing other gases which optically absorb at the same wavelength.

Research is required to determine a suitable wavelength of light to be used and the type of SAM's suitable for a particular type of gas. The main interest in conducting this experimental study was to determine the behavior of various alkanethiol monolayers of different surface energy towards hydrocarbon gases and to find a band of wavelengths sensitive to a gas (propane, methane), with respect to the monolayer used for gas adsorption. In order to accomplish, this spectroscopic ellipsometry and FTIR were used to interrogate the surface (exposed to gas) to determine whether the gas adsorbed on the monolayer and the sensitive wavelength to detect the adsorption.

For the purpose of this study, hydrophobic 1-octadecanethiol $CH_3(CH_2)_{17}SH$ (C-18), and hydrophilic 16− mercaptohexadecanoic acid $HS(CH_2)_{15}COOH$ (COOH) were used. A simple schematic of these SAM's is shown in Fig. 3.1 and 3.2 where the symbolic features are replaced thus: for a monolayer of $CH_3(\ CH_2)_{17}SH$ the functional

tail group is replaced by the methyl group (-CH_3) which is a terminal group that produces low surface energy, and for $HS(CH_2)_{15}COOH$ it is replaced by the carboxylic group (-COOH) which has a high surface energy. When choosing monolayers a major consideration is surface energy. COOH and C-18 lie at opposite ends of the spectrum in terms of surface energy. And it is expected that they will behave differently towards the chosen gases.

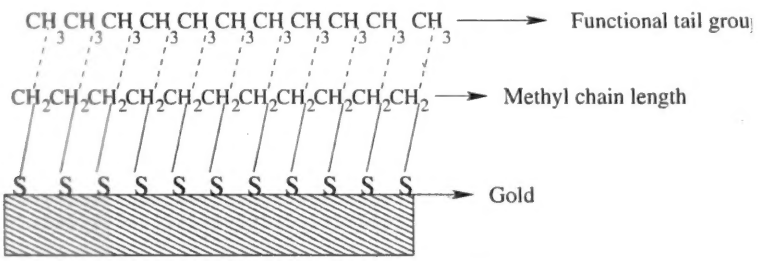

Figure 3.1: Schematic representation of a 1-octadecanethiol self-assembled monolayer adsorbed on a gold metal support.

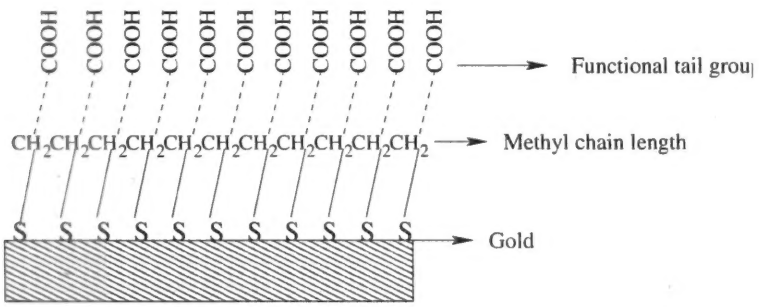

Figure 3.2: Schematic representation of a 1-mercaptohexadecanoic acid self-assembled monolayer adsorbed on a gold metal support.

3.2 Methods and Materials

3.2.1 Materials

Test grade silicon wafers were obtained from Wafer World (West Palm Beach, Fl) with 100 mm diameter. These wafers were sawed into rectangular shapes of about $2.5cm \times 5cm$. Gold (99.999%) and titanium pellets (99.995%) were obtained from Kurt J Lesker (Clairton, PA). Ethanol (100%) was obtained from the Chemistry department, University of Alberta. 1-Octadecanethiol and 16−mercaptohexadecanoic acid were obtained from Sigma-Aldrich and used as received.

3.2.2 Preparation of SAM's

Au/Ti/Si substrates for this experiment were made in an in-house evaporator using the process described in detail in chapter 2. Substrates were prepared by sequentially evaporating titanium (100 Å) and gold (1000 Å) onto silicon wafers in a diffusion-pumped vacuum chamber at 10^{-6} Torr. The layer thicknesses were measured with a quartz crystal monitor (QCM). The chamber was backfilled with air and the substrates used within 48h of preparation. The evaporated surfaces were blown dry with nitrogen gas and then immediately used for the formation of the SAM's. SAM's of C-18 and COOH were prepared by immersing the test pieces into solutions of $CH_3(CH_2)_{17}SH$ or $HS(CH_2)_{15}COOH$ in ethanol for 12h. The resulting surfaces were then rinsed with ethanol and blown dry by nitrogen before use. Propane and methane were obtained from Prax Air in various concentrations.

3.2.3 FTIR

Fourier Transform Infrared (FTIR)was used to characterize the C-18 and COOH monolayers and to observe the changes in the characteristic absorbance peaks of the monolayer before and after exposure to the gas. In the FTIR a sample is interrogated with an infrared (IR) signal. This IR beam can either bounce off (reflectance spectroscopy) or pass through (transmission spectroscopy) the sample and this induces vibrations in the molecules. Energy associated with different bonds is unique and they vibrate giving out radiations which are the signature "fingerprints" of the molecules under investigation. This energy will change the frequency of the IR wave at the detector and thus analyzing the changes in the frequency will provide the information about the molecular bonding thereby providing information about the chemical structure.

The FTIR instrument employed in this experiment is a Nexus 670 with a KBr beam splitter and liquid N_2 cooled MCT/A (mercury-cadmium-telluride) detector. The actual range of detectable signals is 7400-600 cm^{-1}. The FTIR is purged with dry air to minimize interference from water vapor or CO_2. Spectra were obtained with a variable angle specular reflectance unit (PIKE VeeMax model) accessory using S-polarized light (with polarizer angle set at 90°) incident at 70° with respect to the surface normal. The gain was set to 8, resolution to 4 cm^{-1}, and aperture diameter to 32 mm in each measurement. The spectra were acquired over 512 scans from which a background spectrum was automatically subtracted. All the FTIR data presented in this paper is baseline corrected.

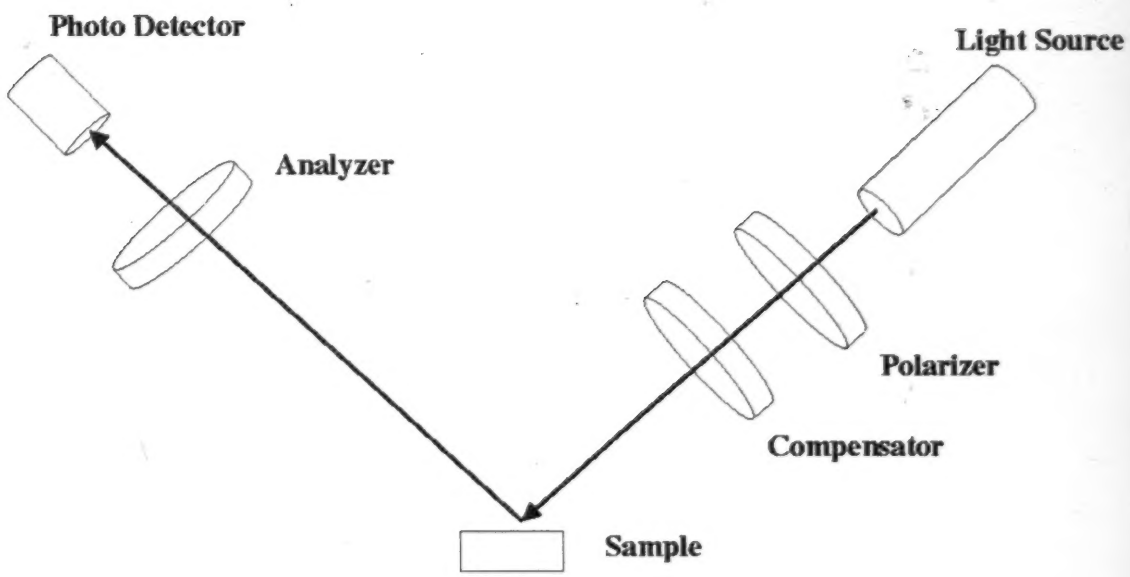

Figure 3.3: Schematic of the ellipsometry setup used for the experiments.

3.2.4 Ellipsometer

All ellipsometric techniques use the physical phenomena where, a linearly polarized light beam is generally elliptically polarized after reflection from a sample surface. The light reflected from the surface has two components [68] polarized perpendicular (s) and polarized parallel (p) to the plane of incidence. Quantitatively it is an optical measurement of the polarization change occurring when light interacts (reflection/transmission) with materials. It is commonly applied to bulk substrates and single or multilayer coatings. The measurement is described by two parameters, Δ

and ψ, that represent phase and amplitude change [69], respectively. Δ and ψ can be related to the complex Fresnel coefficients R_p and R_s of the polarized light by Eq. (4.4) [68].

$$tan(\psi)e^{i\Delta} = \frac{R_p}{R_s} \tag{3.1}$$

Where ψ is the amplitude ratio of the p and s components of the polarized light and Δ is the phase shift of the p and s components of the polarized light [70].

Ellipsometric measurements were performed using a Sopra GESP-5 spectroscopic ellipsometry system. The light beam can be modulated by the rotation of the polarizer, analyzer or of a compensator. For Sopra GESP-5 instrument the measurements were done by linearly polarizing a beam of light from a 75W Xe-arc lamp using a polarizer rotating at 8 Hz and directing it onto the surface at a 75° angle from the surface normal. For this kind of measurements it is a necessity to have a source with well known polarization state. After reflection from the sample, the analyzer is fixed and therefore, it is not necessary to have a detector insensitive to the polarization [71]. To analyze the signal and extract the two components at the double frequency 2P of rotation of the polarizer, Hadamard transformations were used and the signal is integrated after every quarter of the period [71]. The data for $\tan\psi$ and $\cos\Delta$ were collected over the visible (0.3-0.850 μm) and near infrared range (0.9-2.0 μm) using a rotatable analyzer in the tracking analyzer mode.

Also, spectroscopic ellipsometry measures the changes in the intensity after reflection/refraction from the surface and this intensity at the detector is given by Eq.

(3.2) where; I [72], can be described by:

$$I = I_0(\alpha * \cos 2P + \beta * \sin 2P + 1) \tag{3.2}$$

where:

$$\alpha = \frac{\tan^2 \Psi - \tan^2 A}{\tan^2 \Psi + \tan^2 A} \tag{3.3}$$

$$\beta = 2 * \cos \Delta * \frac{\tan \Psi * \tan A}{\tan^2 \Psi + \tan^2 A} \tag{3.4}$$

$$I_0 = \frac{|r_s|^2 |E_0|^2}{2} + \frac{\cos^2 A}{\tan^2 \Psi + \tan^2 A} \tag{3.5}$$

Since α, β and I_0 are functions of $\tan \psi$ and $\cos \Delta$ which are parameters of the physical properties of the material as described by Eq. (3.6), therefore we can relate the intensity to the physical properties by Eq. (3.2). In the above equation A is the analyzer angle and there is no need of reference measurement for the intensity as the coefficients alpha and beta do not depend on the intensity of the lamp.

$\cos \Delta$ and $\tan \Psi$ for a bare gold substrate were measured as a reference after evaporation. Again, the measurements were taken for $\tan \psi$ and $\cos \Delta$ after immersing the substrates into 1-octadecanethiol solution for overnight. Using an ambient-film substrate model for regression with known refractive indices for 1-octadecanethiol and gold, the thickness for C-18 was determined. The refractive index for C-18 was obtained from Sopra GXR grazing reflectometer. The thickness of the adsorbed monolayers were computed using the formula [70]:

$$\tan \psi = \frac{f(n_j, k_j, t_j)}{e^{i\Delta}} \tag{3.6}$$

In Eq:(3.2), n is the refractive index and k is the extinction coefficient of the film, t is

its thickness and the subscript j represents various wavelengths. An average of three measurements were used to calculate the thickness of each sample.

3.3 Gas Exposure Setup

The gas exposure experimental setup is shown in Fig. 3.4 and was designed in-house. A sealed chamber of stainless steel was built and connected to the gas cylinders with Swagelock valves. Gas cylinders with known concentrations 10% of propane and methane in 90% of nitrogen, 20% of propane and methane in 80% of nitrogen and 30% of propane and methane in 70% of nitrogen, respectively were used as obtained from Prax Air.

Experiments were done in the following sequence : first, the optical properties of the SAM's were recorded with FTIR or ellipsometry before being exposed to the gas, then they were exposed to the gas of interest, and again analyzed by FTIR and ellipsometer. It was estimated that to disassemble the gas exposure setup and recover the exposed monolayers for FTIR and ellipsometry analysis took close to 80 seconds. The experiments were performed by varying the pressure and concentration of the gas used. Gas was introduced to the chamber (1) at constant pressure 200kPa and at a variable concentration of the gas, and (2) variable pressure and a constant concentration (20%) of gas. All other experimental parameters such as temperature and humidity were kept constant at laboratory conditions.

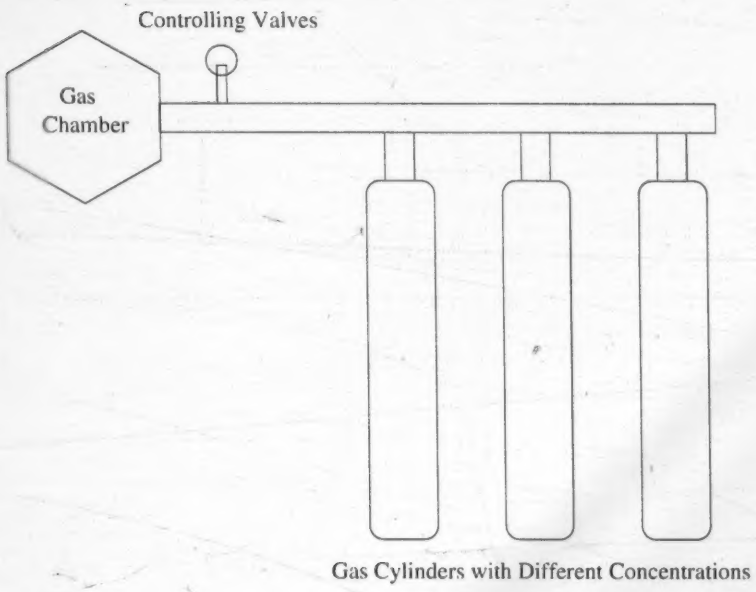

Figure 3.4: Schematic representation of the gas exposure setup used in this experiment.

3.4 Surface Characterization by FTIR and Spectroscopic Ellipsometer

The SAM's were characterized before and after exposure to the test gas. FTIR, spectroscopic ellipsometry and atomic force microscopy (AFM) were all used for the characterization.

3.4.1 FTIR Measurements

In Fig. 3.6, the FTIR spectra for the C-18 monolayer suggests chain orientations consistent with other studies of the same system [73]. The results reflect the anticipated peak positions for the methylene backbones, the symmetric $\nu_s(\ CH_2)$ and asymmetric $\nu_a(CH_2)$ stretching at 2850 cm^{-1} and 2918 cm^{-1}, respectively. The figure also shows the peaks for the symmetric methyl and asymmetric methyl groups at 2878 cm^{-1}

and 2963 cm^{-1}, respectively. This suggests that the monolayers being studied are well-formed with normally packed densities [73] with polycrystalline structure.

FTIR results for COOH are displayed in Fig. 3.7, which shows the typical absorption band spectra for COOH. The results reflect the anticipated peak positions for the methylene backbones: the symmetric $\nu_s(CH_2)$ and asymmetric $\nu_a(\ CH_2)$ stretching at 2851 cm^{-1} and 2919 cm^{-1} respectively. For COOH, the C=O double bond stretch should lie in the range from 1760-1665 cm^{-1}. This expectation is met in our measurements. It is evident from the FTIR analysis that C-18 and COOH are chemically different.

3.4.2 Spectroscopic Ellipsometry

Ellipsometric studies were used to characterize the thickness of the surfaces using a SOPRA GESP-5 variable angle ellipsometer. The measured thicknesses for C-18 and COOH alkanethiol monolayers were 20.4 Å and 18.3 Å which are in good agreement with those reported in literature [74, 73, 75].

3.5 Results and discussions

3.5.1 Results from Elliposmetry

Substrates of COOH and C-18 were exposed to different concentrations of propane and methane at constant pressure and laboratory conditions and analyzed with an ellipsometer to observe if there was any variation in the intensity of the light reflected from the surface before and after exposure. Propane diluted with nitrogen was used in three different concentrations 10%, 20% and 30%, respectively. Methane was used

in 20% concentration. Figure 3.8 shows the variation of intensity with respect to wavelength when C-18 was exposed to propane. As can be seen, there is a difference in the intensity before and after exposure. However, there is no intensity region with respect to the wavelength which shows a consistent relative difference in the intensity reflected/absorbed from the exposed surface. It was expected that with an increase in the concentration of gas used, the relative difference in the intensity reflected from the surface after exposure to the gas should increase. However, the analysis of the spectra gave a result not only inconsistent with this expectation but also without any consistent trend with respect to the different concentrations of the gas used. In Fig. 3.8, from 0.9–1.1 μm the relative difference decreases as we move from 10% to 30% concentration of gas, but from 1.1–1.4 μm the relative difference is constant. From 1.45–1.65 μm the relative difference decreases; however, from 1.7 μm to 1.9 μm it first increases slightly for the surfaces exposed to 10% and 20% and then it again decreases for 30%. For the methane exposed to C-18 in Fig. 3.8, the difference in the intensity reflected is relatively small as compared to propane.

Spectra for the COOH SAM exposed to propane is given in Fig. 3.9. As can be seen, for COOH exposed to 10% propane the relative difference in the intensity before and after exposure is considerable. However, in case of 20% and 30% the error is large enough to make the results ambiguous. For COOH exposed to methane in Fig. 3.9 the difference in the intensity reflected before and after exposure is considerable. However, the overall trend is similar to that of propane with the only difference being in the intensity reflected across the spectrum.

3.5.2 Results from FTIR

Since the results from ellipsometry were not definitive, the next logical step was to use FTIR to determine the change in the absorbance spectra of the SAM's after exposure to the gas of interest. Experiments were carried out systematically by exposing C-18 and COOH to varying concentrations of gas at a constant pressure (200 kPa) and room temperature. In a second step the pressure was changed and the concentration was kept constant at 20% (20% Propane and 80% Nitrogen).

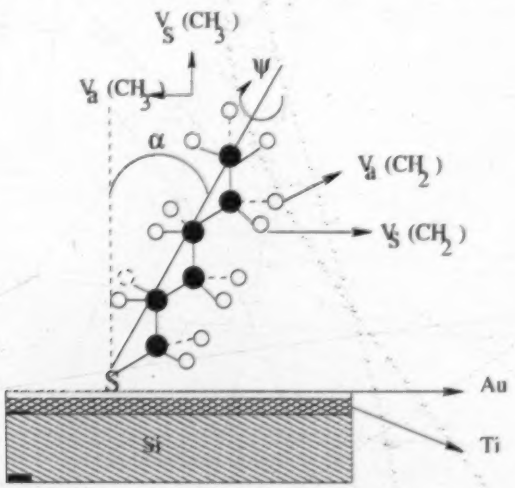

Figure 3.5: Schematic illustration of an alkanethiolate adsorbate that is tilted at $30°(\alpha)$ from the surface normal and twisted $0^0(\beta)$ around its molecular axis.

In Fig. 3.5 arrows indicate the transition dipole moments for the following stretching modes : $\nu_s(CH_3)$, $\nu_a(CH_3)$, $\nu_s(CH_2)$, and $\nu_a(CH_2)$. The intensities of the infrared bands for these transition dipole moments depend on their projection along the surface normal. The differences in the intensity of the absorbance spectra of the FTIR indicate different canted orientations of the methylene on these surfaces with the surface (Au) normal. The tilt for alkanethiolate SAM's on gold is 30° [76], which is a

result of the packing arrangement of the monolayer on the metal (Au) surface. An increase in the tilt angle results in a corresponding increase in the methylene peaks in the spectra, whereas a decrease in the tilt angle reduces the peak height [73]. This explanation of the behavior of the peak height of CH_2 with respect to the tilt angle of the hydrocarbon chain helps in interpreting the FTIR results.

Apart from propane, SAM's were also exposed to methane to determine if there is any change in the spectra when using a different gas. Figure. 3.10 shows gas phase propane and methane FTIR spectra. For both propane and methane [77], the region of interest is concentrated between 2850–3025 cm^{-1}.

Figure .3.11 shows the FTIR spectra of C-18 taken after exposure to propane and methane. As can be seen, C-18 exposed to various concentrations of propane and methane shows little change in the CH_3 absorbance peak and no distinct peaks for methane in the 2850–3025 cm^{-1} range. However, in Fig. 3.12 peaks are observed at 3016 cm^{-1} for C-18 and C-18 exposed to propane at 200 kPa. These small peaks can be attributed to the residual ethanol left after the wash of C-18 coated Au with 100% ethanol solution. Other than these peaks the FTIR spectra for C-18, and C-18 exposed to propane looks relatively similar. There is a small difference in $\upsilon_a(CH_2)$ and $\upsilon_s(CH_2)$ for C-18 exposed to propane and methane as the peak height for $\upsilon_a(CH_2)$ and $\upsilon_s(CH_2)$ has increased relative to the unexposed C-18. This difference is very small and can be attributed to an increase in the tilt angle of the methylene backbone after exposure to propane gas which results in a corresponding increase in the methylene peaks in the spectra. This small variation can also be attributed to the differences in

the gold substrates and/or atmospheric contamination. Similarly there is a change in the $\upsilon_a(CH_2)$ and $\upsilon_s(CH_2)$ peaks for C-18 (Fig. 3.12) exposed to propane at different pressures. However, these changes are similar to those observed in Fig. 3.11 for propane and methane, and for the symmetric and antisymmetric CH_3 absorbance peak there is no change.

It is evident from the results that their is no strong indication of the adsorption of propane or methane on C-18 monolayer. The changes in $\upsilon_a(CH_2)$ and $\upsilon_s(CH_2)$ peaks after exposure are not relatively large enough to conclude that the change is due to the gas exposure. Figure. 3.13 shows all the spectra of COOH taken after exposure to propane and methane. As can be seen, for wave-numbers between 2850–3025 cm^{-1}, no distinct absorbance peaks for CH_3 and CH_4 were observed. However, there is a difference in the absorbance peaks (2950 cm^{-1} and 2918 cm^{-1}) of COOH exposed to propane and methane relative to unexposed COOH. This decrease in the peak height of $\upsilon_a(CH_2)$ and $\upsilon_s(CH_2)$ can be attributed to the decrease in the tilt angle of the methylene backbone relative to the surface normal on Au surface or it can be due to the fact that their is a thin film of the gas on the monolayer which is decreasing the intensity of infrared reaching the monolayer molecules their by reducing the peak height. In the next phase of the experiment, COOH was exposed to a propane (20% propane + 80% nitrogen mixture) at different pressures. From Fig. 3.14, it is clear that there is a change in the absorbance peaks of COOH at 2950 cm^{-1} and 2918 cm^{-1} after exposure.

It is evident from these results that the trends observed for the $\upsilon_a(CH_2)$ and

$\upsilon_s(CH_2)$ peaks for propane (constant pressure and variable pressure) and methane are similar. Furthermore, there is a decrease in the peak height of $\upsilon_a(CH_2)$ and $\upsilon_s(CH_2)$ after exposure to the gas molecules; presumably due to a change in the tilt of the backbone or it can be due to the fact that their is a thin film of the gas molecules on the monolayer which is decreasing the intensity of infrared reaching the monolayer molecules their by decreasing the peak height. However, the tilt in this case is opposite to that observed in C-18 and is much more pronounced.

3.6 Conclusions

The sensitivity of the self assembled monolayers of C-18 and COOH to hydrocarbon gases has been experimentally . Spectroscopic ellipsometry was used to measure the change in the intensity of the light that was reflected from the SAM's before and after exposure to the gas. From the experimental study, it can be concluded that C-18 and COOH exposed to propane and methane exhibit an overall shift in the intensity. However, the results fail to reflect any definitive band of wavelength which can be used to differentiate between propane and methane. For C-18 exposed to propane and methane the only difference that is observed is in the reflected intensity across the spectrum, and moreover this difference is not consistent giving a ambiguous trend. For COOH exposed to propane, the instrument error is large enough to make the results ambiguous. However, for COOH exposed to methane the relative difference in the intensity is large enough to demand further investigation.

Further investigation was carried out with FTIR, and it was observed that no

distinct absorbance peaks were observed for methane in case of C-18 and COOH. Also, no change in the CH_3 peak was observed in case of C-18 after exposure to propane and there was no distinct peak observed for CH_3 in case of COOH. However, changes in the peaks of $\upsilon_a(CH_2)$ and $\upsilon_s(CH_2)$ for C-18 and COOH were observed. These change were relatively negligible for C-18 as compared to COOH.

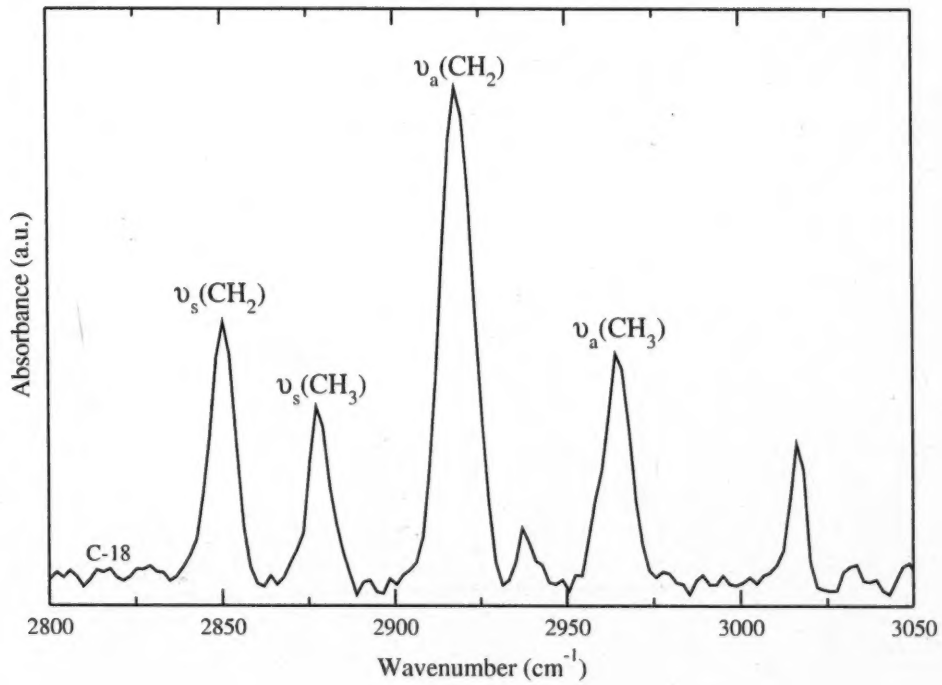

Figure 3.6: Typical FTIR spectra of 1-octadecanethiol monolayer

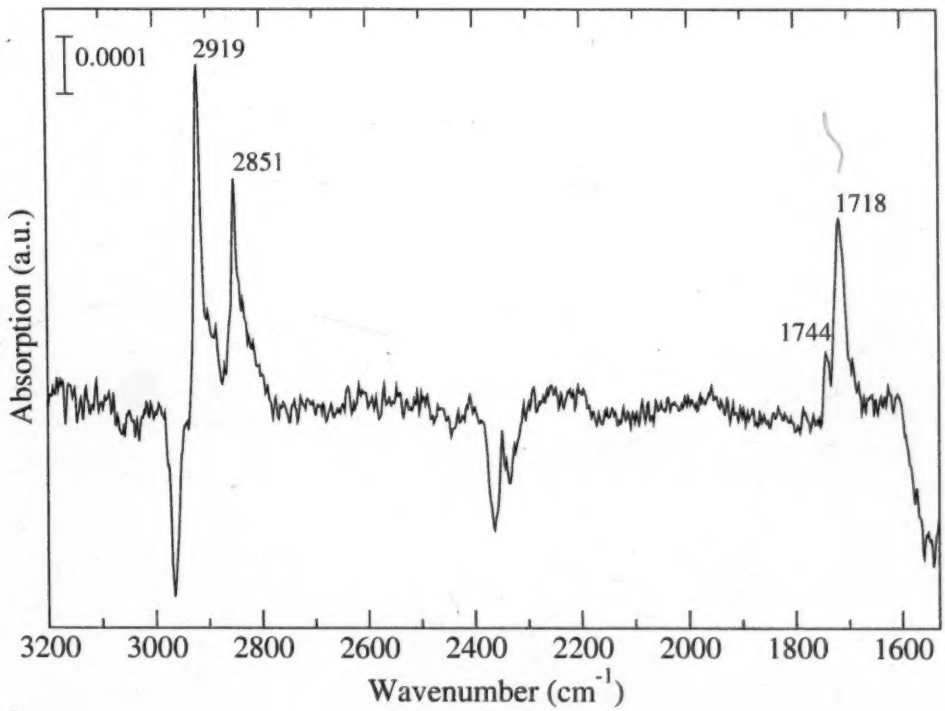

Figure 3.7: Typical FTIR spectra of 1-mercaptohexadecanoic acid

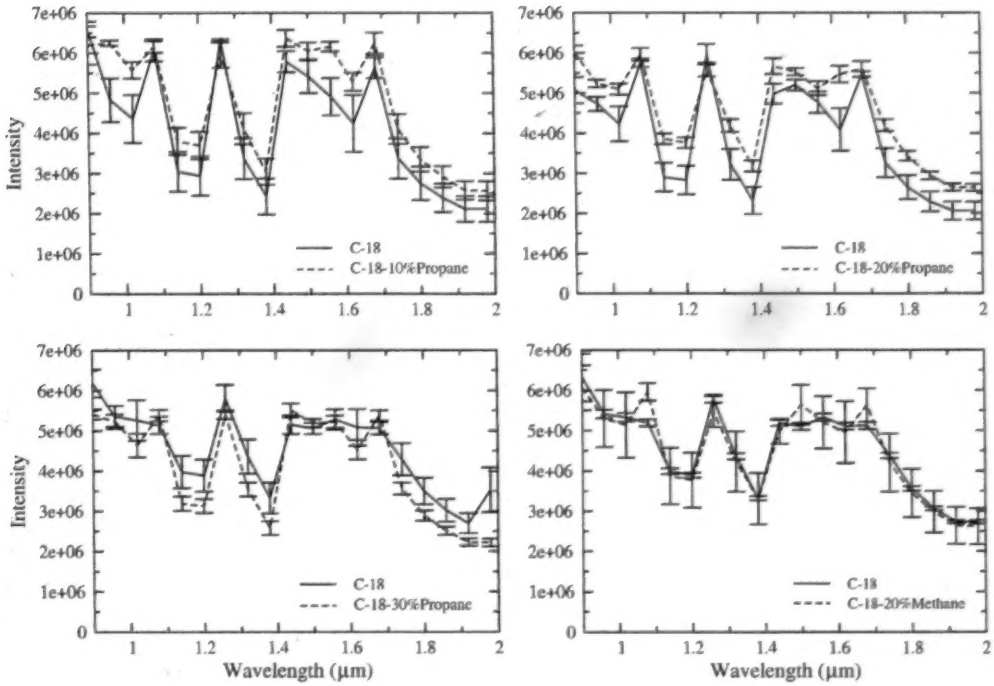

Figure 3.8: Variation in intensity with wavelength for C-18 before and after exposure to propane and methane

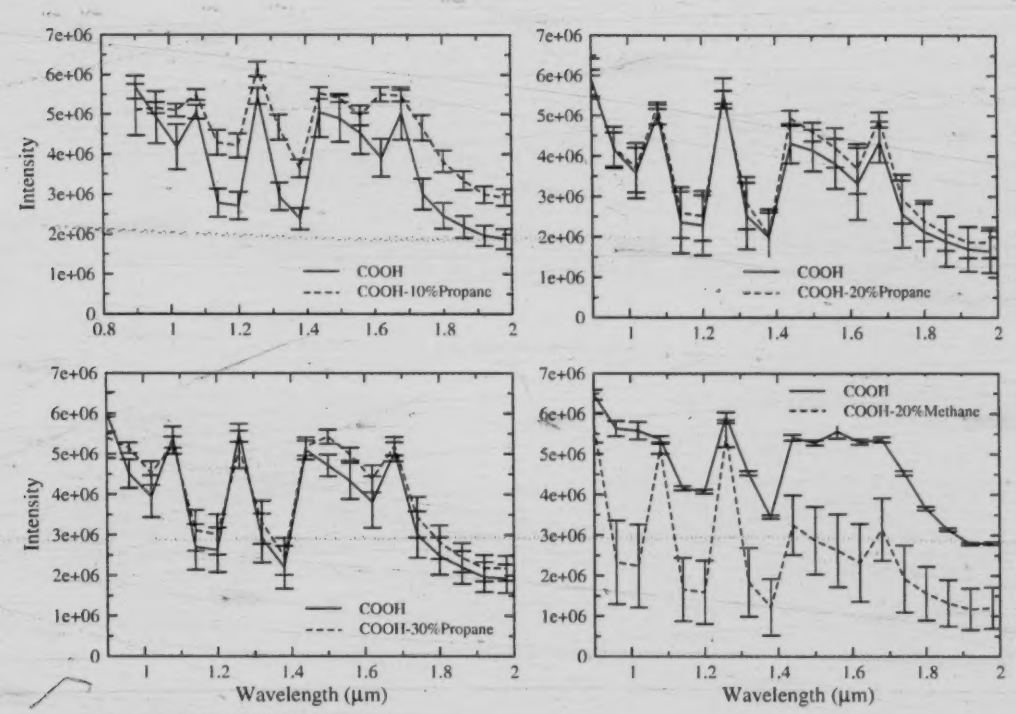

Figure 3.9: Variation in intensity with wavelength for COOH before and after exposure to propane and methane.

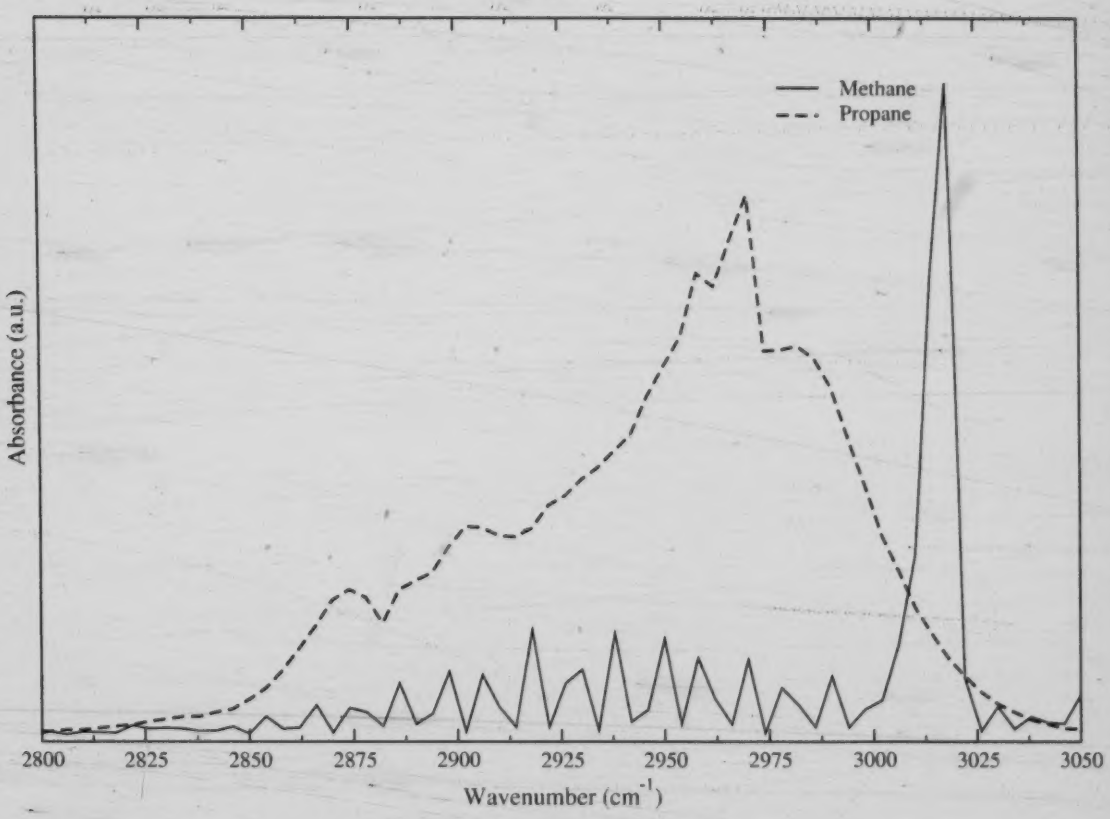

Figure 3.10: FTIR spectra of propane and methane in the gaseous phase (data taken from http://webbook.nist.gov/chemistry).

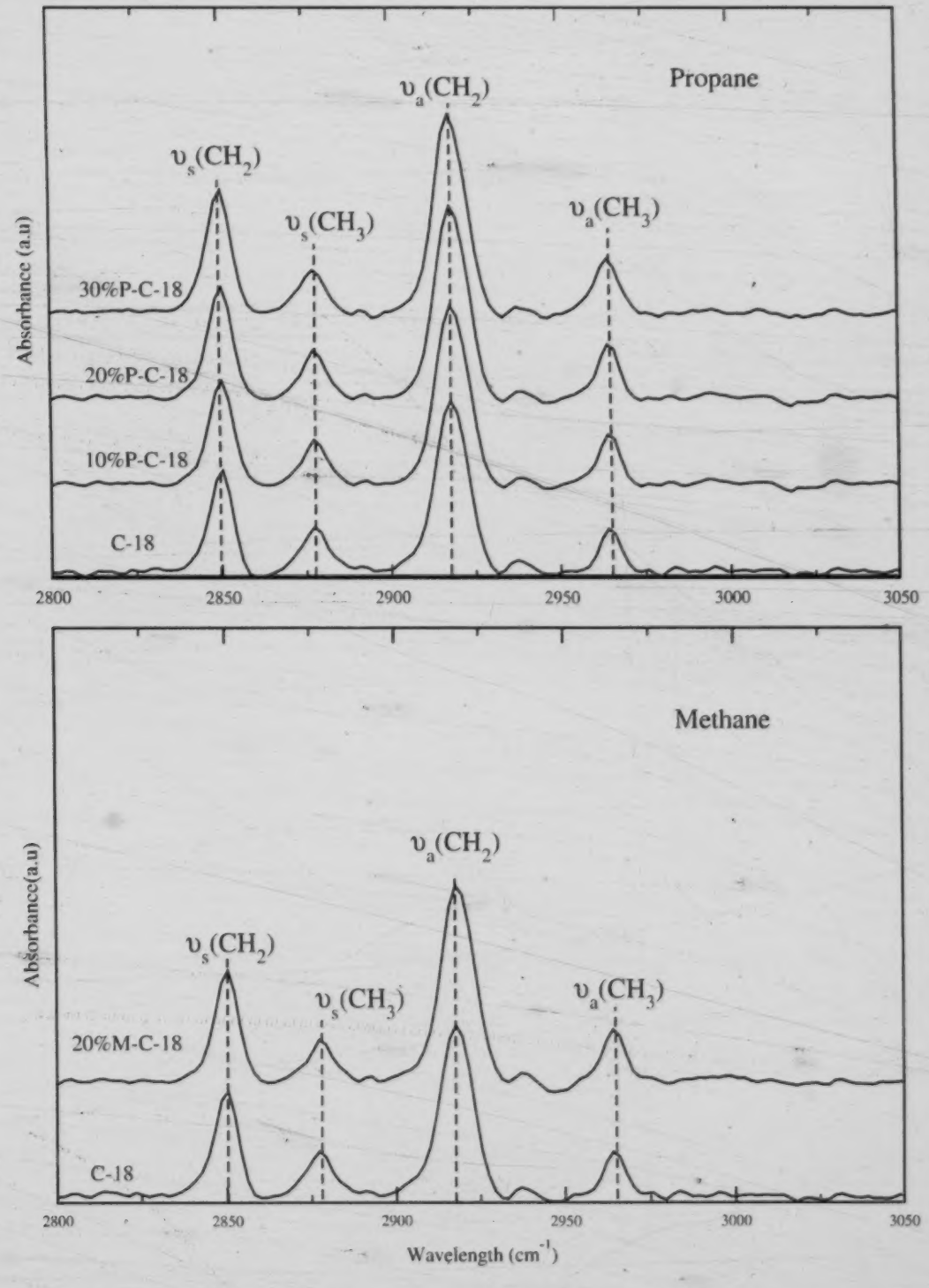

Figure 3.11: FTIR spectra of C-18 self-assembled monolayers after being exposed to different concentrations of propane and methane at constant pressure (200 kPa) and temperature (295 K).

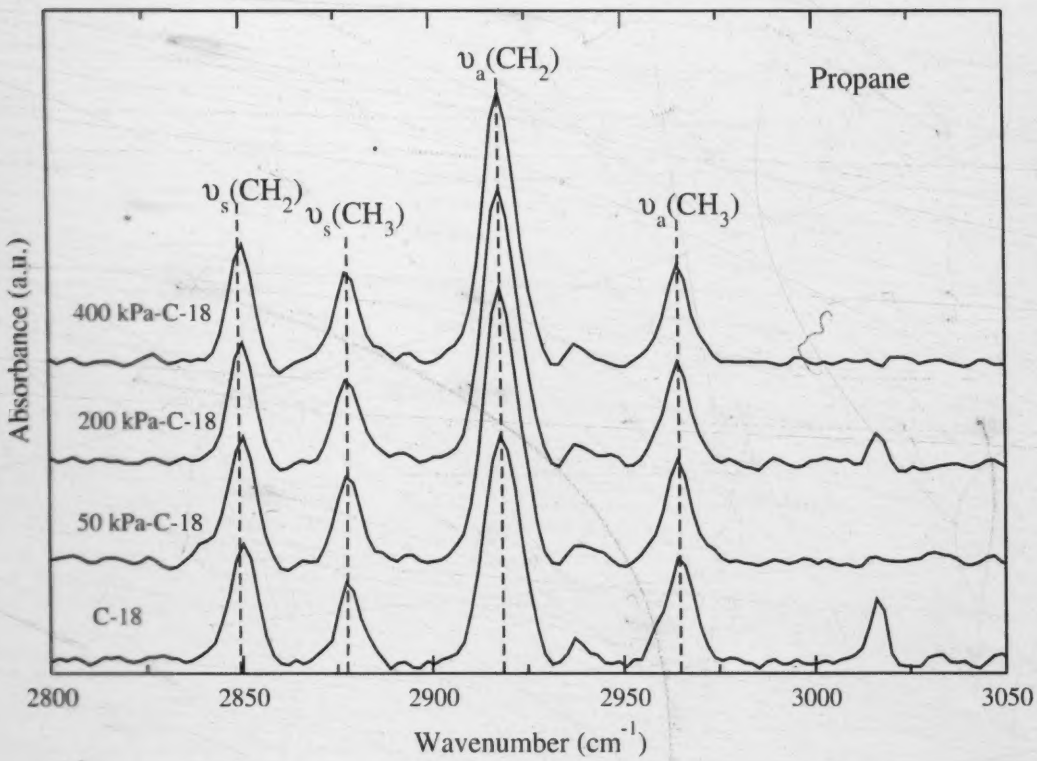

Figure 3.12: FTIR spectra of C-18 self-assembled monolayers after being exposed to 20% propane at different pressures and constant laboratory temperature of 295 K.

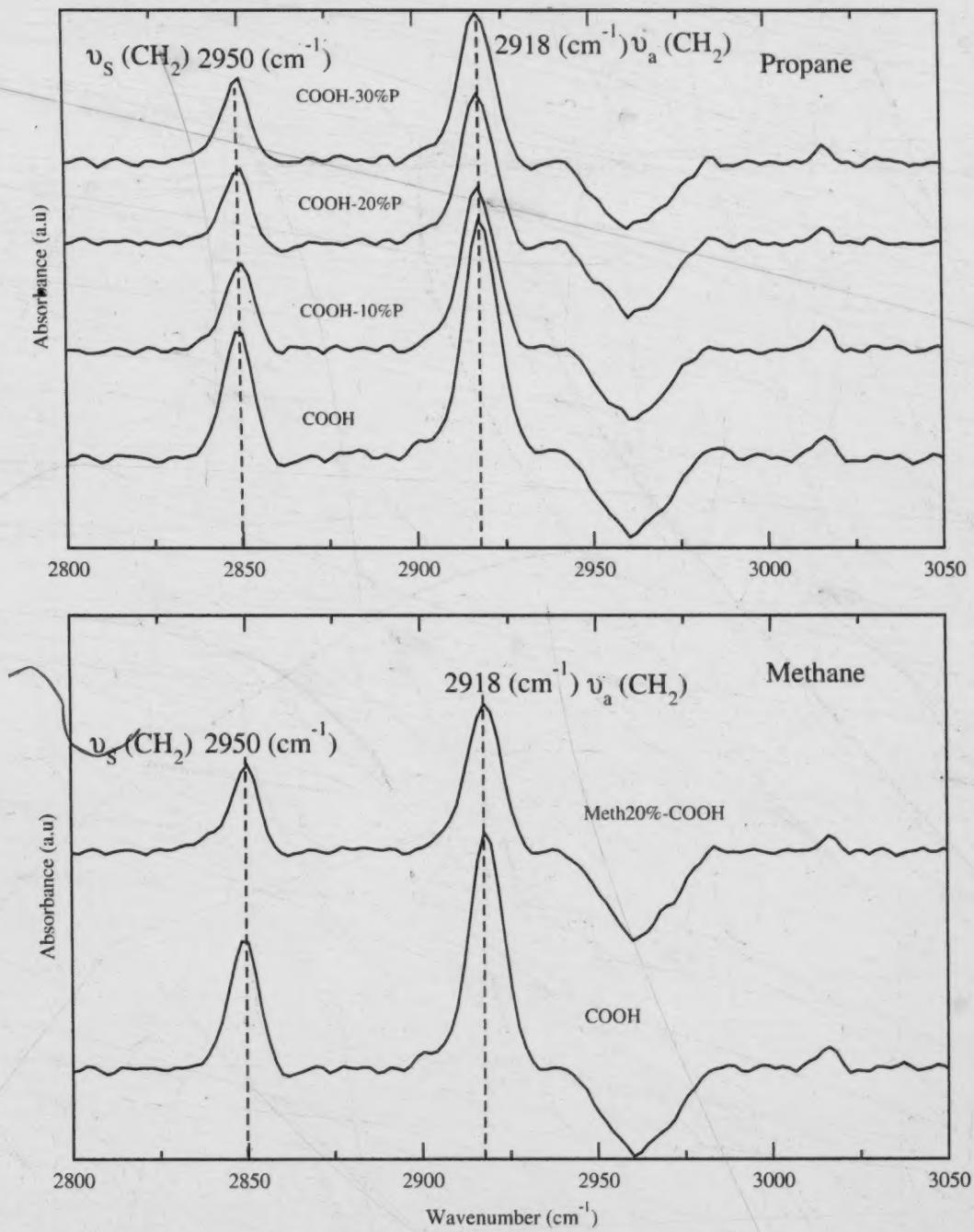

Figure 3.13: FTIR spectra of COOH self-assembled monolayers after being exposed to different concentrations of propane and methane at constant pressure (200 kPa) and temperature (295 K).

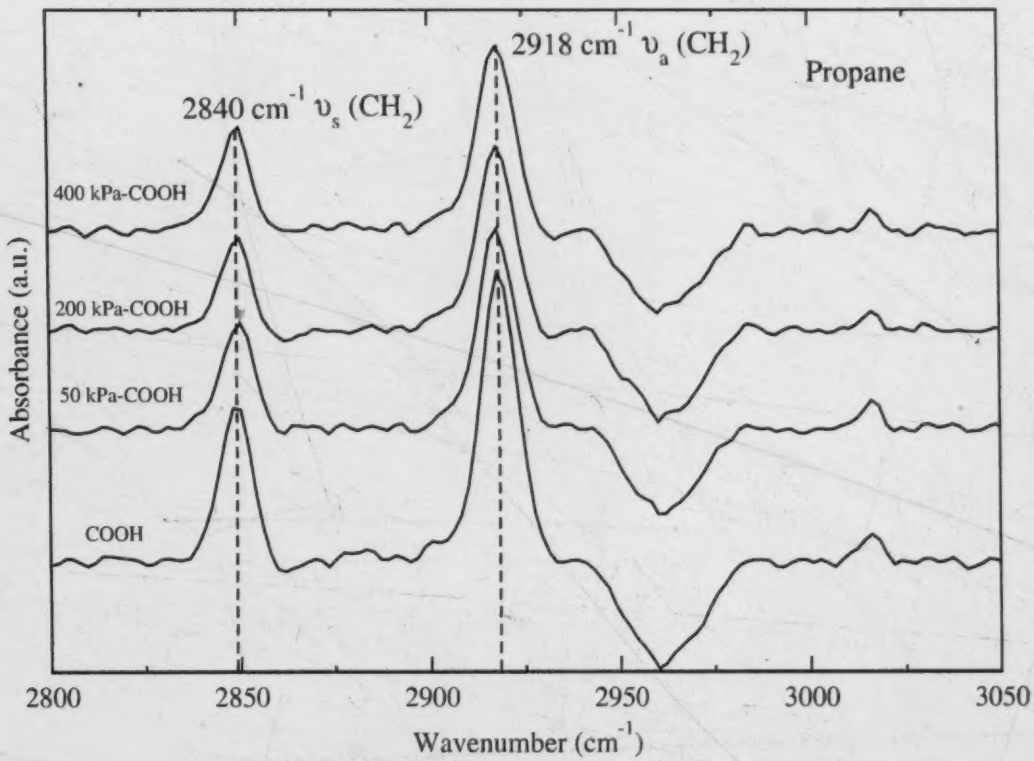

Figure 3.14: FTIR spectra of COOH self-assembled monolayers after being exposed to 20% propane at different pressures and constant temperature of 295 K.

Chapter 4

Spectroscopic Ellipsometry for Characterization and Concentration Measurement of Proteins Immobilized on SAM's.

4.1 Introduction

During the last decade, the scientific community has witnessed tremendous research activity aimed at the realization of optical sensors for the measurement of biological and chemical quantities. Optical sensors, using the adsorption spectrum were first developed for the measurement of CO_2 and O_2 concentration [25]. Since then a large variety of optical methods have been used in chemical and biological sensing, like surface plasmon resonance [78, 79], ellipsometry, interferometry (modal interferometry in optical waveguide structures, white light interferometry spectroscopy) and spectroscopy (luminescence, Raman, fluorescence).

Development of large-scale biosensor arrays composed of highly miniaturized signal transducer elements that enable the real-time and parallel monitoring of multiple species is an important driving force in biosensor research. This is particularly

significant in high-throughput screening applications such as drug discovery and proteomics research where many thousands of ligand-receptor or protein-protein interactions must be rapidly examined. In these situations it is necessary to utilize sensor platforms that have as many desirable characteristics of optical biosensors as possible.

Several techniques have been used for protein identification like mass spectrometry [52], protein structure-NMR [53], X-ray crystallography [54, 55] and light spectroscopy. Spectroscopic ellipsometry [80] in the past has been used as a noninvasive optical technique in the visible (0.270– 0.800 nm) and near infrared (NIR) range (0.825–2.0 nm) of the electromagnetic spectrum for the characterization of thin films [81]. It is possible with this technique to determine the optical response of the surface under consideration and to gain important information about its physical microstructure, such as the possible presence of analytes. The goal of this experimental study is to determine whether two different proteins can be distinguished using ellipsometry. The idea is to find a sensitive wavelength at which the optical response of the particular protein is unique and furthermore, to measure the changes in the optical intensity and constants by ellipsometry and relate these changes to the concentration of the specimen under investigation.

The ideal analytical method for studying the interaction of complex biological media with surfaces should : (1) allow the detection of the interaction in situ, (2) provide kinetic and thermodynamic information about the process and avoid the need for the covalent modification of analyte, (3) use small amounts of material, (4) have a high signal to noise ratio that allows the detection of sub monolayer

quantities of material, and (5) have high specificity for individual structures [82]. No single technique currently meets all these criterions. In the past, gold substrates have been used for immobilizing biological samples to measure the concentration of the molecules using FTIR [83]. Unfortunately, gold is not a practical platform to design sensors intended for biological applications because of its high surface energy which favors absorbtion of contaminants from the atmosphere thus contaminating the sample. This problem can be overcome by designing and synthesizing surfaces using SAM's of alkanethiols [33, 34, 35] on gold and silver.

Two SAM's have been employed for this study; hydrophobic 1-octadecanethiol (C-18), and hydrophilic 16-Mercaptohexadecanoic acid (COOH). The reason for choosing C-18 (highly hydrophobic) and COOH (highly hydrophilic) is their unique surface properties because of their low and high surface energies respectively. They are at the opposite end of the surface energy spectrum, which makes them interesting candidates for investigating the adhesion behavior of biological samples with surfaces and how it effects the concentration measurement. Albumin (HSA) from human serum (> 98.0% purity) has been used as a model biological sample for concentration measurements. For protein characterization 1-octadecanethiol $CH_3(CH_2)_{17}SH$ (C-18) self-assembled monolayer on gold was used. The reason for choosing C-18 was its high hydrophobicity, which enabled the formation of a uniform and homogenous residue of protein. Apart from HSA, Fibrinogen (FIB) from human plasma (50% protein content) was used as sample protein for characterization study. These experiments were carried out at room temperature and pressure to mimic typical sensing conditions.

4.2 Experimental section

4.2.1 Protein Deposition Method

FIB and HSA were obtained from Sigma-Aldrich and used as received. HSA and FIB 15% (15mg of HSA/FIB in 100 ml of phosphate buffer solution) solutions were prepared in phosphate buffer using deionized ultra filtered water (DIUF). Sample preparation consisted of depositing a drop of 0.50 ml of each protein onto the surface of a C-18 monolayer on a Au/Ti/Si substrate and leaving it to dry at room temperature and pressure. The shape of the solid residual of the protein left after the evaporation of the buffer was circular with an average surface diameter of 7 mm.

However, this preparation is plagued by a major inconvenience. The protein residue left after the evaporation was of non-uniform thickness. To reduce the effect of this thickness variation, the protein solution was left to vibrate on a table during the evaporation process. The frequency of the vibrating table was set to 45 Hz. At this frequency, the amplitude of the mechanical vibrations induced in the drop by the table was resonant [83], thus optimizing the mixing of protein in the evaporating phosphate buffer solution and resulting in a fairly uniform thickness and relatively homogeneous residual. This procedure was followed for all the protein samples prepared for data collection using ellipsometry.

4.3 Discussions and Results

4.3.1 Interpretation of Ellipsometric Data

Light intensity reflected from bare Au substrate was measured using ellipsometry and a similar measurement was performed on a C-18 coated Au substrate. Subsequently, measurements were also taken of C-18/Au/Ti/Si samples on which FIB or HSA proteins were deposited. In order to compare the response of protein to different optical sources, measurements were done in both the visible and NIR wavelengths of the electromagnetic spectrum.

Figures 4.1, 4.2, 4.3, and 4.4 show the variation of intensity at each wavelength, collected at the ellipsometer detector after reflection of the incident light from C-18, Au, HSA and FIB in the visible and NIR region of the electromagnetic spectrum. The differences in the curves clearly point toward the uniqueness of the different surfaces being examined. Furthermore, since the difference in the intensity reflected from C-18 and Au (Figures. 4.1, 4.2, 4.3, and 4.4) is relatively small, either can be used as a control surface. However, it is highly desirable to use C-18 because of its inertness to atmospheric contamination as compared to Au [3].

It was anticipated that the protein layer would reduce the light intensity reflected from the Au and C-18 surfaces. However, contrary to this, the intensity reflected from the surface coated with HSA (Fig. 4.2) was higher in the wavelength range of 0.4-0.45 μm. Furthermore, for FIB the light reflected at the 0.42 μm wavelength is equivalent to that reflected from Au and C-18. In Figures 4.1 and 4.2 the data exhibits a clear difference between the proteins (HSA and FIB), C-18, and Au surfaces

in the wavelength region 0.3–0.45 μm. However, after 0.45 μm the data is scattered across the wavelength rendering it ambiguous for protein identification. Hence, only the wavelength range from 0.3–0.45 μm is promising for HSA and FIB identification.

As can be seen that the Fig. 4.3 and 4.4 show the variation of the intensity with respect to the wavelength in NIR region of the electromagnetic spectrum. In each figure, the data points are quite smooth and systematically distributed across the NIR wavelength. The intensity variation trend across the NIR wavelength is nearly similar for C-18, Au, HSA, and FIB with the only difference being in the relative amount of intensity reflected from each surface. However, the intensity of the light reflected from SAM's with HSA and FIB on them yields two unique curves in the NIR region. The curves are different from each other, clearly distinguishing between the two different proteins examined.

In Figures. 4.1, 4.2, 4.3 and 4.4 respectively, it is interesting to note that the relative difference in intensity between all 4 experiments for HSA and FIB in the visible and NIR region of the electromagnetic spectrum varies. This variation can be explained by the variations in the thickness of the deposits. These differences in thickness cause the measurements to change from one experiment to another. As can be seen Fig. 4.5 shows the average of the four different spectra for HSA and FIB in the visible region. The spectra have been averaged to enhance the signal-to-noise ratio and to minimize the error in the measurement caused by the variation in the thickness of the deposits. This averaged spectra clearly shows the difference between the two proteins.

4.3.2 Relationship between Thickness and Concentration

The relationship between thickness and concentration has already been derived by Garcia et al [83], in which the deposited drop was considered to be a perfect hemisphere of radius, r, having protein of concentration, C, dissolved homogeneously in it. The total protein mass can be calculated by multiplying volume with concentration:

$$m = \frac{2C\pi r^3}{3} \tag{4.1}$$

The protein residual left after the evaporation of the water was observed to be cylindrical in shape with radius, R, thickness, d, and apparent density of, ρ_0. Therefore, the total mass of protein can be calculated as follows:

$$m = \rho_0 d\pi R^2. \tag{4.2}$$

Since the mass of the protein is not changing during the evaporation process we can equate Eq. (4.1) and Eq. (4.2) to obtain a linear relationship between the deposited thickness, d and the concentration, c in the original solution.

$$d = \frac{2r^3}{3R^2\rho_0}C. \tag{4.3}$$

The relationship between thickness, d, and concentration, C, can be assumed to be linear in Eq. (4.3) by considering that the variation in the drop size radius r, and the solid residual radius R, and the density of the deposit, ρ_0, is negligible between different samples. Certainly it was found during the experimentation that equal solution volumes gave equally sized drops for a given surface, thus making the thickness independent of radius. Substrate temperature, composition, and the concentration of

the protein in the water are the experimental parameters that effect the evaporation and thus effect the density. These were kept constant by maintaining the laboratory temperature at 295 K thereby minimizing the residue density variability. Substrates used in this study were prepared using standard techniques developed in our lab and described in detail in the previous chapters.

The issue of the concentration inhomogeneity was minimized by using the method of sample preparation described earlier in this chapter to minimize the variation in density. Samples were prepared by a successive deposition method. To vary the concentration of the samples, a drop with a given initial concentration, C_0, was deposited on a pre-existing solid residual of the protein. This preexisting solid residual of the protein dissolved each time a new drop was deposited, thus leaving a residual with twice the initial concentration. It can be assumed that after the new deposit has been grown, the concentration of the residual is not the initial concentration but some final concentration achieved after the dissolution of the initial residual.

4.3.3 Variation in Intensity with respect to the Change in Concentration

As can be seen Fig. 4.6 shows the intensity collected at the ellipsometer detector after reflection from different concentrations of the protein deposited on a C-18 monolayer. It is clear from the figure that even for the same amount of protein concentration, the intensity curves are different. This difference is much more pronounced at the beginning of the deposition; however, as the thickness of the deposited protein grows and becomes more uniform, the curves become much more consistent and reflective

of the increase in concentration. For 0.5 ml and 2 × 0.5 ml the difference in the intensity is not that striking and the intensity curves overlap each other for the entire range of the near infrared (NIR) spectrum. However, between 2 × 0.5 ml and 3 × 0.5 ml the difference is quite evident until 1.15 μm after which the intensity curves start overlapping. The overlap in this case is relatively small as compared to that in the case of 0.5 ml and 2 × 0.5 ml. For 4 × 0.5 ml there is a striking difference with respect to the other concentration curves.

As can be seen Fig. 4.7 shows the averaged curves for the various concentrations of the protein on C-18. It is evident from the figure that until 1.2 μm the intensity curves are quite distinct and they reflect the change in concentration from 0.5 ml to 4 × 0.5 ml; however, this change in intensity is not a linear representation of the change in concentration which is inconsistent with what was expected. For the rest of the wavelength range the curve for 0.5 ml overlaps with 2 × 0.5 ml; whereas the curves for 2 × 0.5 ml, 3 × 0.5 ml and 4 × 0.5 ml are distinct, and show a relatively linear variation with the change of concentration.

Figure 4.8 shows the intensity collected at the ellipsometer detector after reflection from different concentrations of the protein deposited on a COOH monolayer. It was expected that with the increase of the protein deposit, the intensity reflected from the surface would decrease. As can be seen, the curves for the different concentrations of protein are quite complex and they deviate from the expected trend in comparison to C-18. The reason for this deviation can perhaps be attributed to the high surface energy and consequent larger surface spreading of the protein solution on a COOH

surface compared to that on C-18 [73]. Due to this spreading, the deposited protein does not have a uniform thickness on COOH as compared to a surface coated with C-18.

Figure 4.9 shows the averaged out curves for various concentrations of the protein on COOH. It further strengthens the assertion about the inconsistency observed in the COOH curves. In the wavelength region from 0.96–1.02 μm and 1.75–1.9 μm, the intensity measured from 2 × 0.5 ml, 3 × 0.5 ml and 4 × 0.5 ml reflects the change in the protein concentration, and this change is relatively linear with respect to the concentration. However, the light intensity reflected from 2 × 0.5 ml, 3 × 0.5 ml and 4 × 0.5 ml is more than that of 0.5 ml which is inconsistent with the expected result.

Variation of tanΨ with respect to the change in concentration

Variation of $tan\Psi$ with respect to the change in concentration was determined in order to compare tan Ψ relative to intensity. The basis of this comparison stems from the fact that both intensity and tan Ψ are measured at the same time and are derived from the same samples.

$$\tan \Psi = \frac{f(n_j, k_j, t_j)}{e^{i\Delta}} \tag{4.4}$$

In the above equation tan Ψ is dependent on n, k, film thickness and the Δ. Where n is the reflective index and k is the extinction coefficient. It is clear from the above relation that the tan Ψ is directly proportional to the change in the thickness of the surface, therefore, a change in tan Ψ can be related to the change in concentration by Eq. (4.3). Figure 4.10 shows the variation of tan Ψ collected from a variety of samples of protein deposited on C-18 monolayer with respect to wavelength. As can

be seen, tan Ψ varies with the change in concentration of the protein. Moreover, for the same amount of the protein concentration, the tan Ψ measurement is different and varies from one sample to another. The reason for this variation is the non-uniform protein deposition as has already been explained; however, the relative difference in the averaged tan Ψ measurement, shown in Fig. 4.11, reflects the changes in the concentration. Moreover, it can be seen that tan Ψ curves for 2 × 0.5 ml, 3 × 0.5 ml and 4 × 0.5 ml are evenly spaced over the 0.9 μm - 2.0 μm wavelength range and show a relatively consistent variation with the change in concentration as compared to 0.5 ml.

Figure 4.12 shows the variation of tan Ψ collected from protein deposited on COOH monolayer with respect to wavelength. As can be seen, until 1.05 μm, the tan Ψ curves for 0.5 ml, 2 × 0.5 ml, and 3 × 0.5 ml are clearly different, whereas, the 4 × 0.5 ml curve overlaps with that of 3 × 0.5 ml. In Fig. 4.13 the same measurement has been averaged and the result clearly reflects the change in the concentration. However, the relative difference between tan Ψ curves for different concentrations is not as much reflective of the change in the concentration as was the case for C-18.

A comparison of the intensity and tan Ψ results for both C-18 and COOH reveal that tan Ψ is a better parameter for concentration measurement. This confidence in tan Ψ stems from the fact that it is relatively insensitive to the variations in surface inhomogeneity as compared to the intensity. Furthermore, it can be seen from Figures. 4.8 and 4.12 that tan Ψ measured on COOH shows a consistent trend as compared to the intensity, even though both parameters were obtained simultaneously from the

same samples.

4.4 Re-usability

4.4.1 Experimental Section

Self-assembled monolayers of C-18 and COOH are quite robust and resistant to atmospheric contamination as compared to bare gold. To get a qualitative idea of the reusability of C-18 and COOH monolayer surfaces, were exposed multiple times to a test protein. After each exposure, the C-18/Au/Ti/Si and COOH/Au/Ti/Si substrate was treated with a highly ionic solution of KCl and NaCl and a phosphate buffer solution with very high pH to remove the protein and restore the SAM. In Fig. 4.14, 1st treatment refers to the treatment of monolayer after its first exposure to protein and IInd treatment refers to the treatment of the same monolayer after its second exposure to the protein. This procedure was repeated keeping the experimental conditions consistent.

4.4.2 Analysis with FTIR

After each treatment infrared spectra were collected and compared to determine if any deterioration occurred in the C-18 monolayer. Figure 4.14 shows the spectra of C-18 and COOH before and after treatment. As can be seen, peak heights for the methyl end group (symmetric $\nu_s(CH_3)$ and asymmetric $\nu_a(CH_3)$ stretching at 2878 cm^{-1}, 2963 cm^{-1}) and methylene backbone, (symmetric $\nu_s(CH_2)$ and asymmetric $\nu_a(CH_2)$ stretching at 2850 cm^{-1} and 2918 cm^{-1}) are deteriorating after each treatment compared to the original C-18 monolayer. In the case of COOH, there is a

deterioration in the peaks at 2919 cm^{-1} and 2840 cm^{-1}, respectively. The change in COOH is relatively small in comparison to C-18. This shows that the surface adhesion between the protein and the COOH monolayer is less than that of the protein and C-18 monolayer. Thus it can be concluded that COOH is a better surface than C-18 in terms of reversibility.

4.5 Conclusion

We have experimentally studied a method to detect proteins by measuring the light intensity reflected from thin solid residuals left on a $CH_3(CH_2)_{17}SH$ monolayer using ellipsometry and measure the concentration of biological samples by measuring changes in light intensity and optical properties of the thin solid residuals left on a $CH_3(CH_2)_{17}SH$ and $HS(CH_2)_{15}COOH$ monolayer using ellipsometry.

Experiments for the protein characterization were done in the visible and NIR regions of the electromagnetic spectrum. It was discovered that the difference in the measured reflected intensity is most sensitive to the distinguishing chemical features of the protein samples at 0.42 μm wavelength in the visible region. However, in the case of the NIR region two curves clearly separating the proteins were obtained. But in NIR region their is no specific region distinguishing two proteins. The curves looked similar except for the difference in the intensity.

Experiments for concentration measurement were done in the NIR region of the electromagnetic spectrum. It was concluded that the measured reflected intensity is representative of the change in concentration on a C-18 surface in comparison to

COOH. However, for COOH the intensity measured after 2 × 0.5 ml and 3 × 0.5 ml and 4 × 0.5 ml does not give a consistent trend and the curves are scattered. Furthermore, it was observed that $tan\Psi$ is a better parameter than intensity to measure the change in protein concentration for both C-18 and COOH. The relative difference in $\tan\Psi$ measured from protein on C-18 monolayer is better able to reflect the change in concentration in comparison to the $tan\Psi$ measured from the protein on COOH monolayer. From FTIR results, it can be concluded that the COOH surface is a better choice in terms of reversibility than C-18. It can be presumed from these results that the C-18 is a good surface for concentration measurement and COOH is a better choice due to reversibility. However, both of these characteristics are highly desirable in a system designed for concentration measurements therefore, it is important to achieve a balance between them. This balance may possibly be achieved by using monolayers with surface energies which fall in the range between that of C-18 and COOH.

These results not only open a range of possible applications of protein detection and concentration measurement by ellipsometry but with additional research in the future it may lead to the miniaturization of the ellipsometric setup for clinical purposes. This concept also holds promise in the early detection of some types of cancers which occur due to protein mutation.

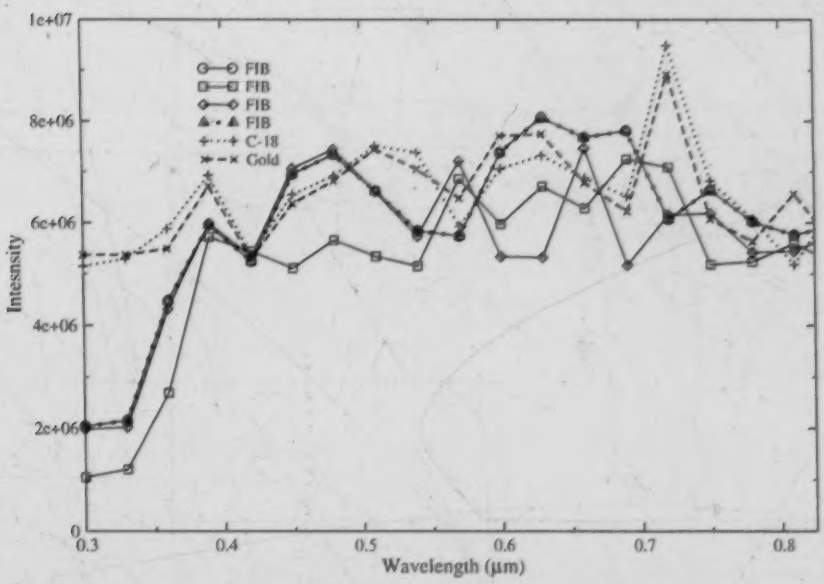

Figure 4.1: Ellipsometry results showing the reflected intensity in the visible region for different samples of FIB deposited on C-18 and reference C-18 and gold.

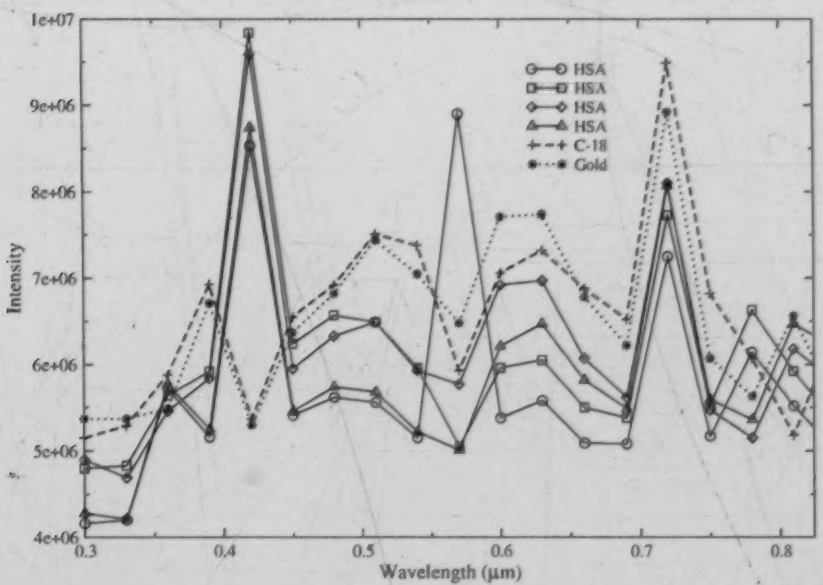

Figure 4.2: Ellipsometry results showing the reflected intensity in the visible region for different samples of HSA deposited on C-18 and reference C-18 and gold.

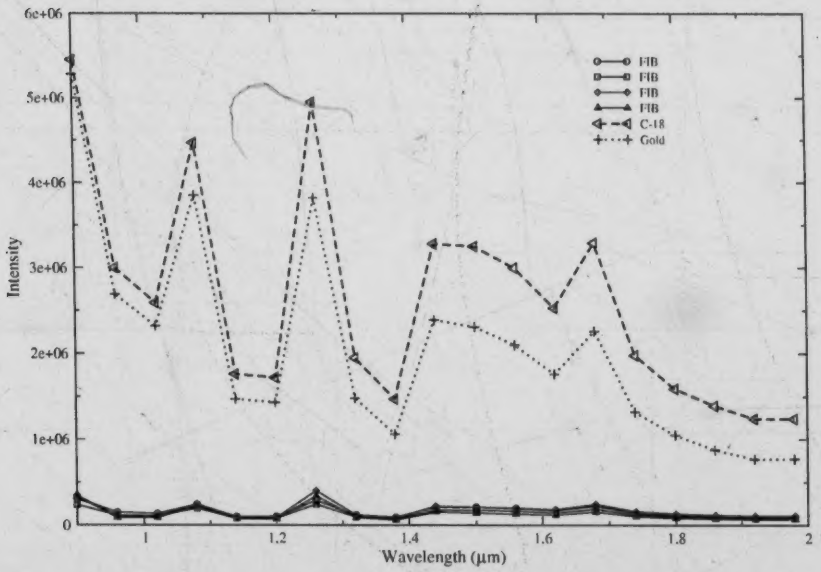

Figure 4.3: Ellipsometry results showing the reflected intensity in the NIR region for different samples of FIB deposited on C-18 and reference C-18 and gold.

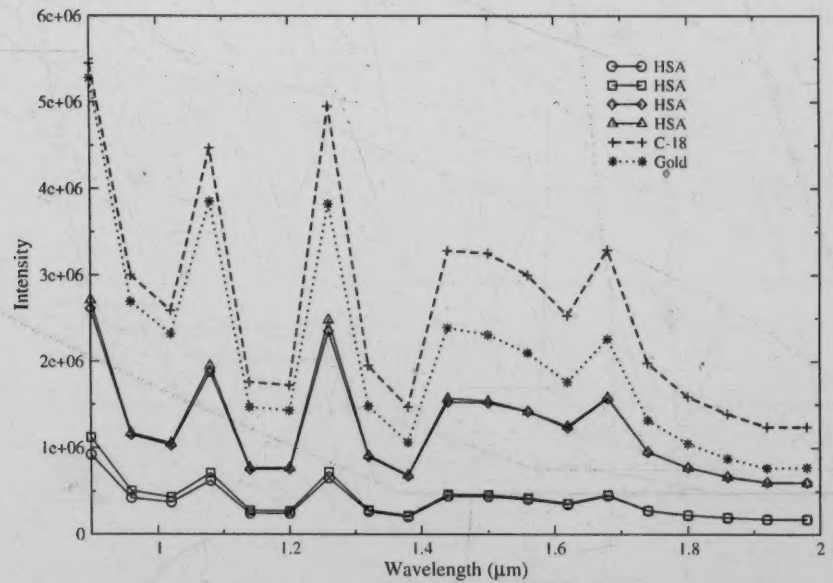

Figure 4.4: Ellipsometry results showing the reflected intensity in the NIR region for different samples of FIB deposited on C-18 and reference C-18 and gold.

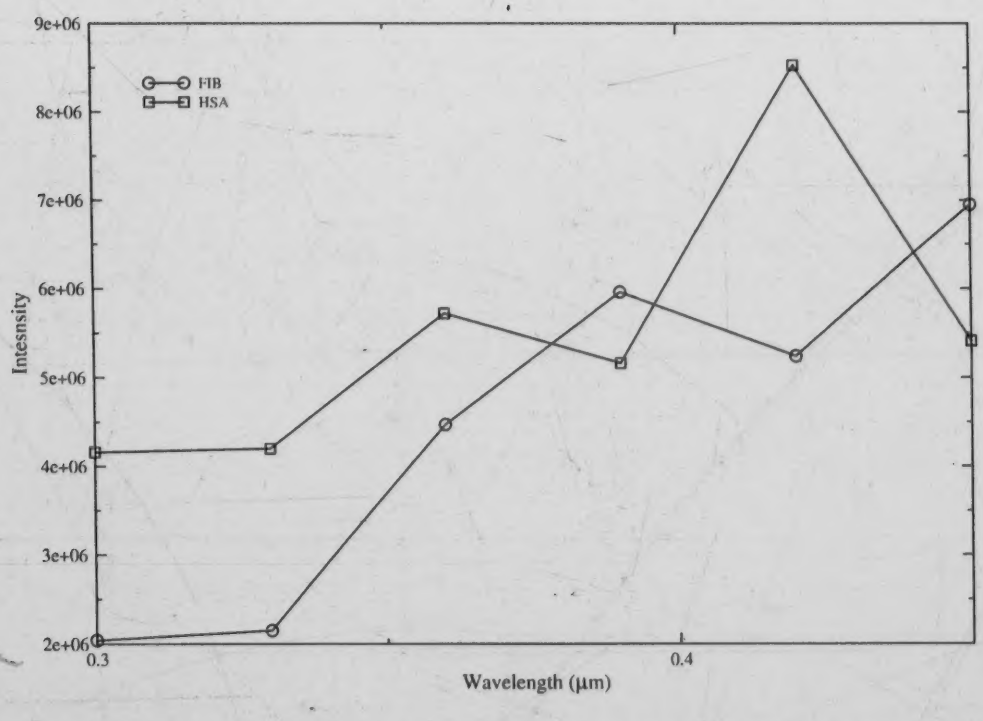

Figure 4.5: Comparison of the average intensity Vs wavelength between FIB and HSA in visible region.

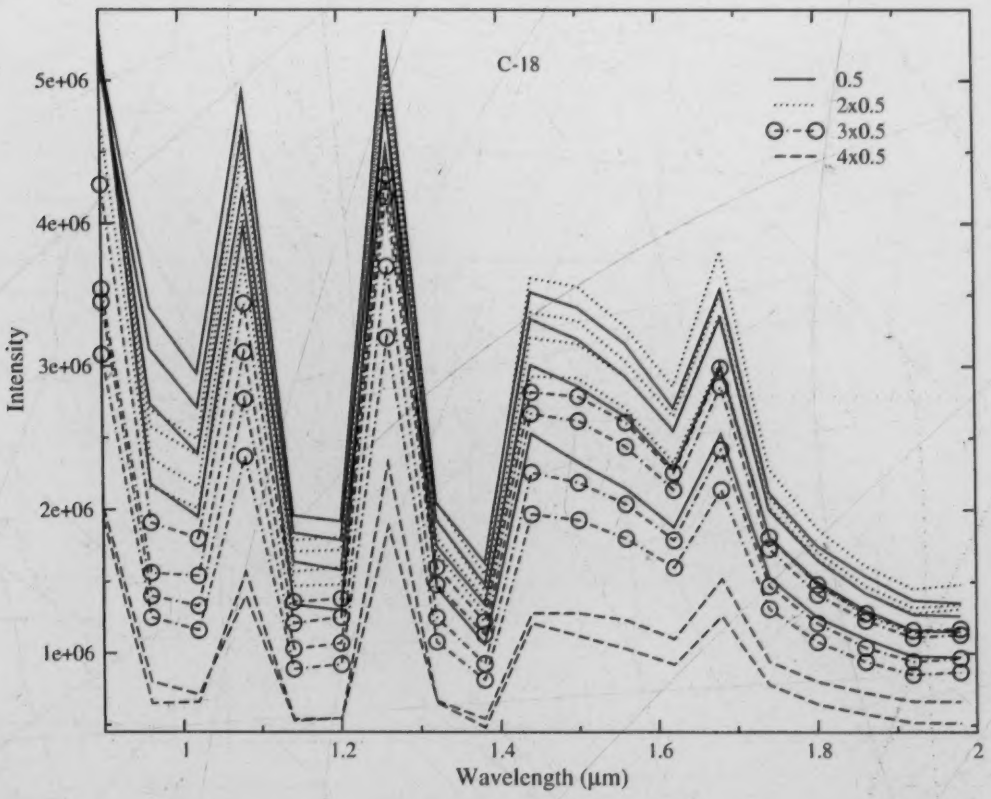

Figure 4.6: Ellipsometry results showing the reflected intensity in the NIR region with respect to the change in the concentration of the HSA protein deposited on C-18 monolayers on Au/Ti/Si substrate for various samples at 4 different nominal concentrations.

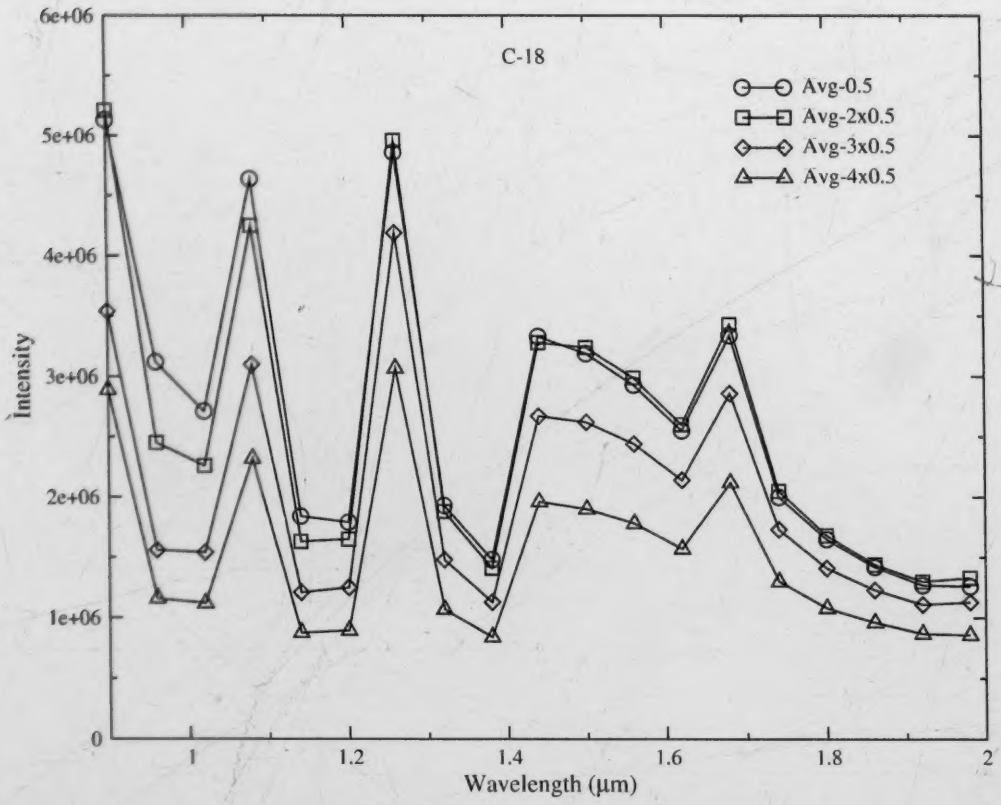

Figure 4.7: Ellipsometry results showing the average change in the reflected intensity in the NIR region with respect to the change in the concentration of the HSA protein deposited on C-18 monolayers on Au/Ti/Si substrate for various samples at 4 different nominal concentrations.

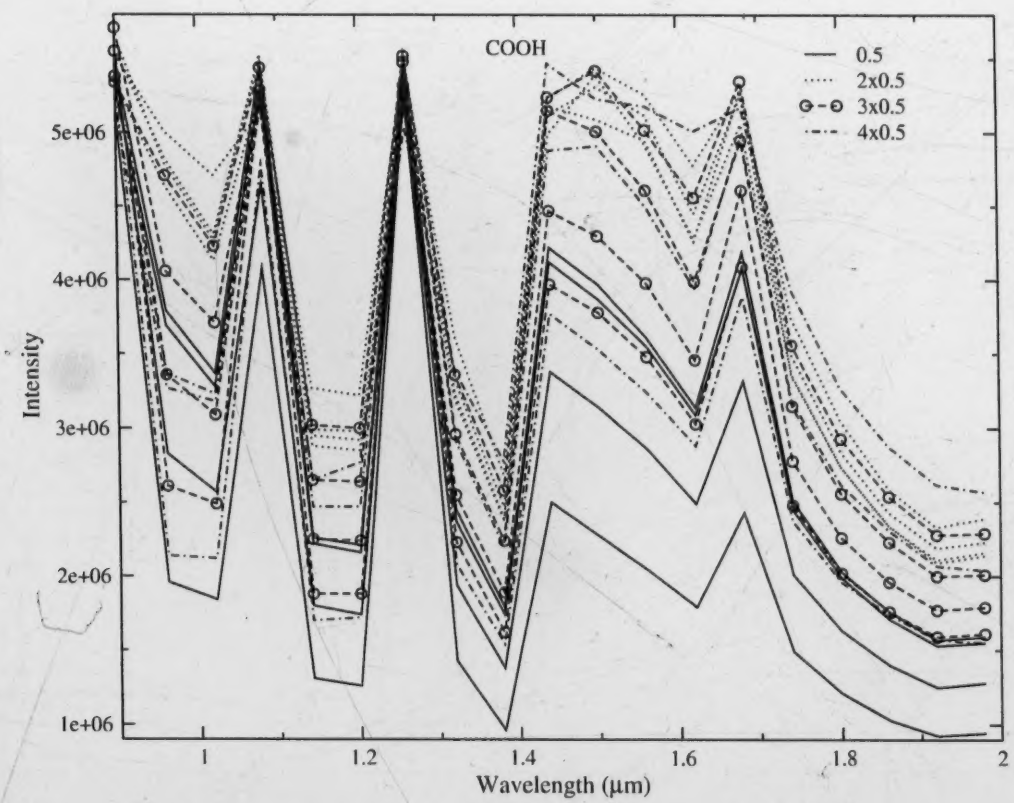

Figure 4.8: Ellipsometry results showing the reflected intensity in the NIR region with respect to the change in the concentration of the HSA protein deposited on COOH monolayers on Au/Ti/Si substrate for various samples at 4 different nominal concentrations.

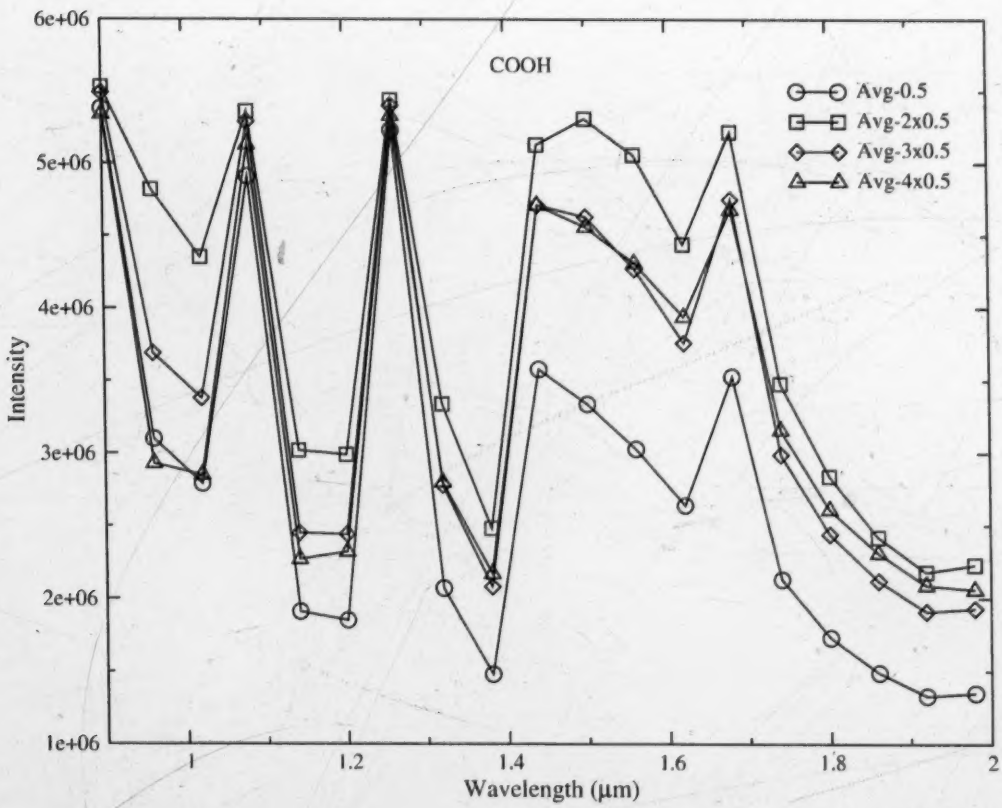

Figure 4.9: Ellipsometry results showing the average change in the reflected intensity in the NIR region with respect to the change in the concentration of the HSA protein deposited on COOH monolayers on Au/Ti/Si substrate for various samples at 4 different nominal concentrations.

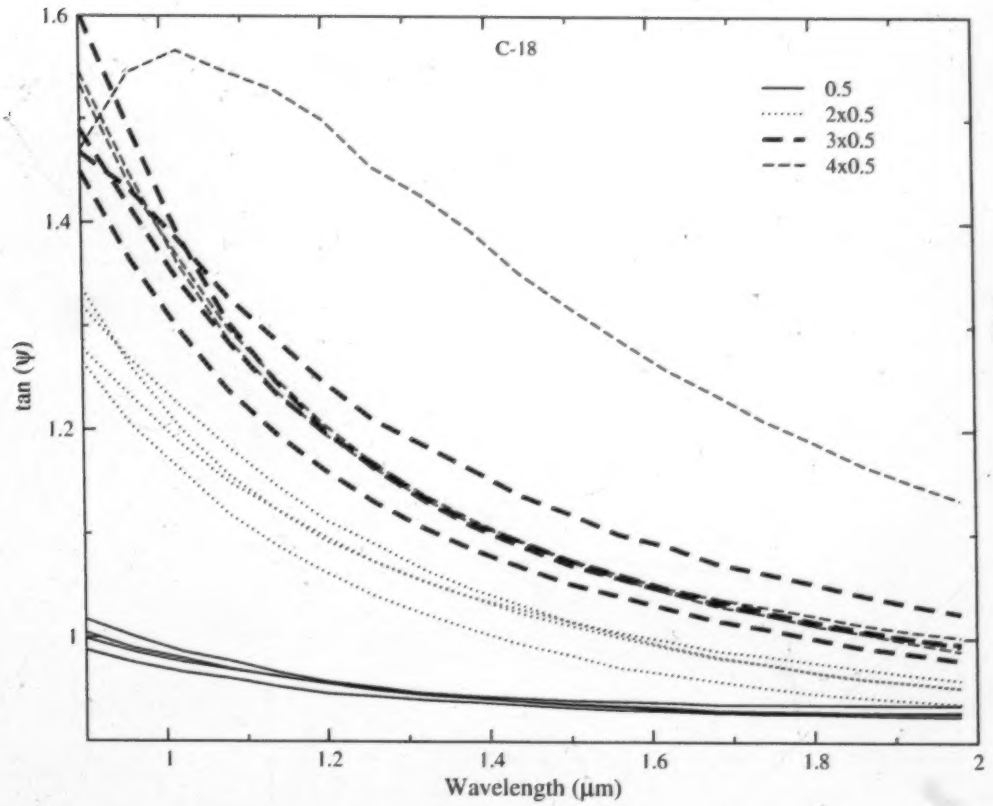

Figure 4.10: Change in $tan\Psi$ with respect to the variation in concentration of the protein deposited on C-18 monolayers on Au/Ti/Si substrate for various samples at 4 different nominal concentrations.

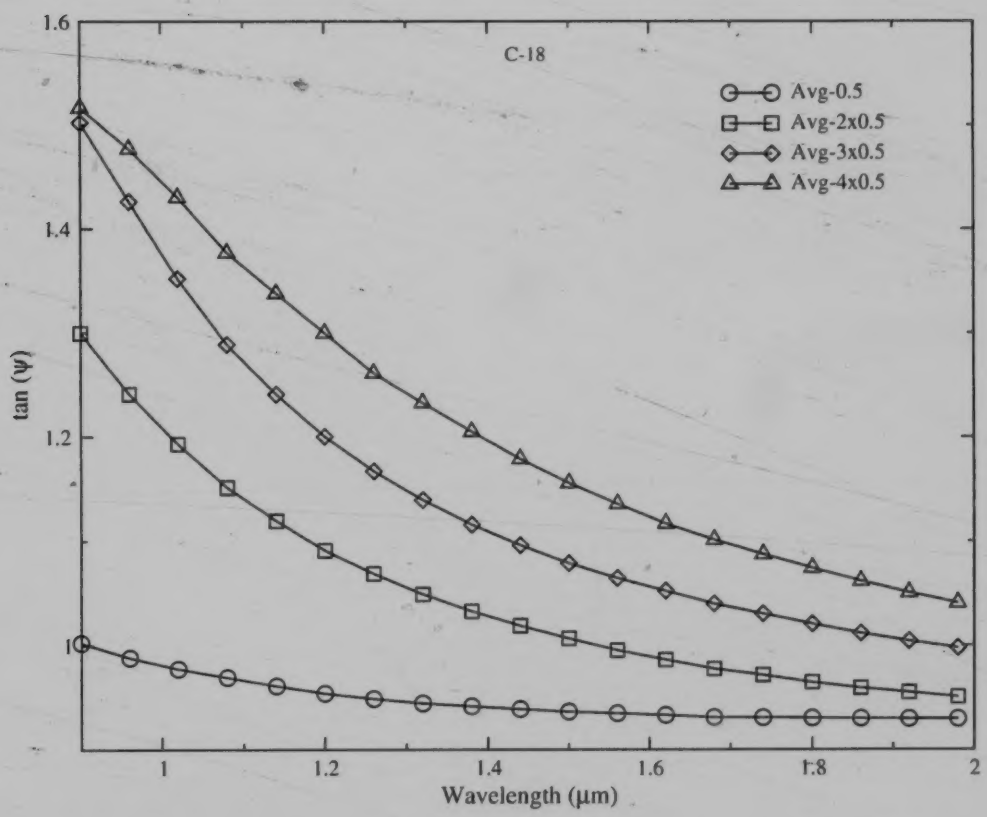

Figure 4.11: Average change in tanΨ with respect to the variation in concentration of the protein deposited on C-18 monolayers on Au/Ti/Si substrate for various samples at 4 different nominal concentrations.

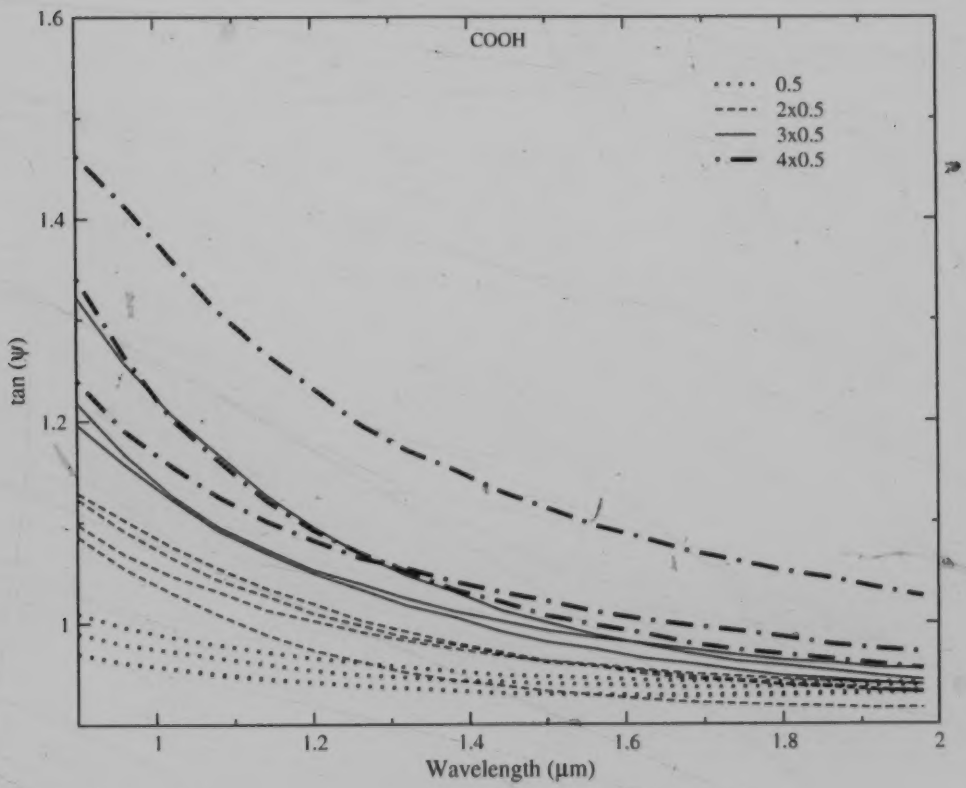

Figure 4.12: Change in tanΨ with respect to the variation in concentration of the protein deposited on COOH monolayers on Au/Ti/Si substrate for various samples at 4 different nominal concentrations.

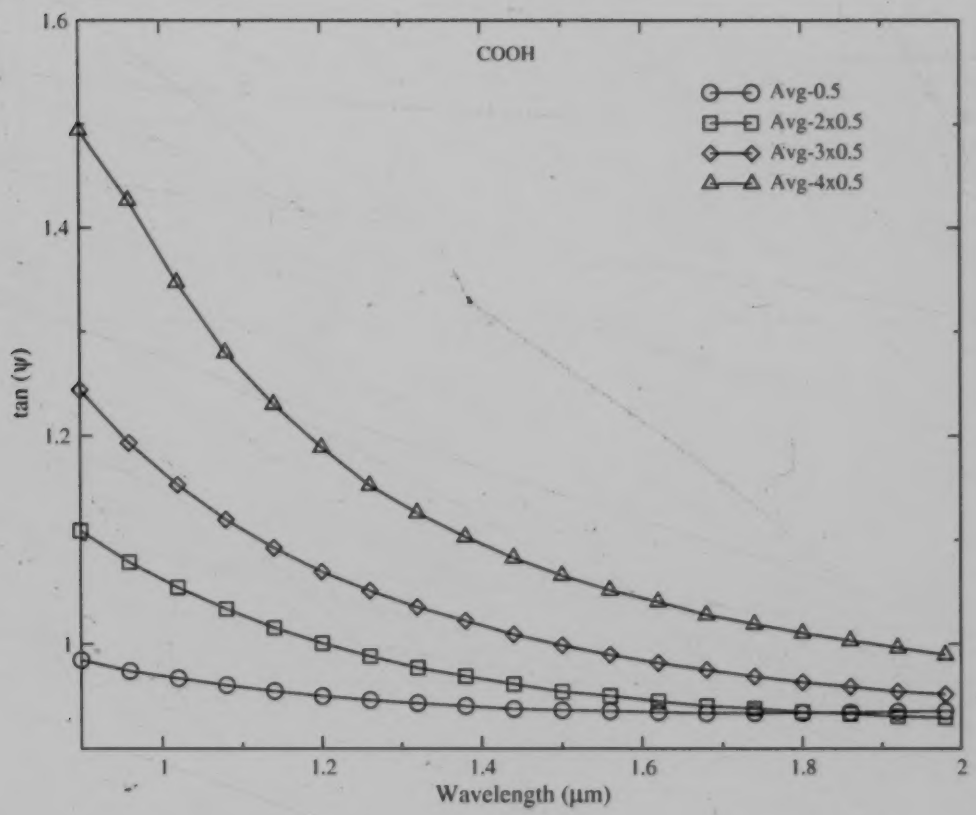

Figure 4.13: Average change in tanΨ with respect to the variation in concentration of the protein deposited on COOH monolayers on Au/Ti/Si substrate for various samples at 4 different nominal concentrations.

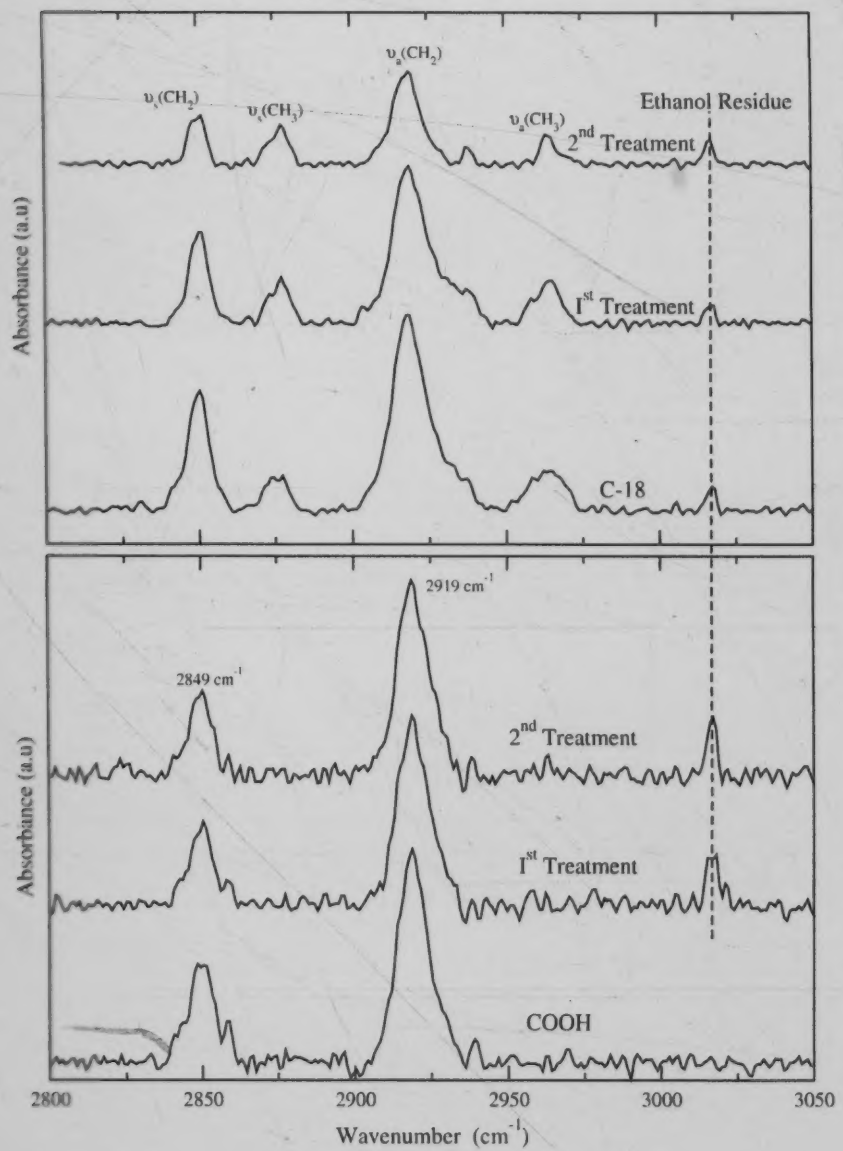

Figure 4.14: Comparison of FTIR spectra's collected after treating the protein deposited C-18 and COOH substrate with highly ionic solution of (KCl and NaCl) and a high pH buffer solution.

Chapter 5

Summary and Future Direction

Summary and future directions can be grouped into two sections according to the experiments that I have done.

5.1 Use Of SAM's for Hydrocarbon Gas Sensing

Using experimental techniques I have looked into the sensitivity of self assembled monolayers of C-18 and COOH to hydrocarbon gases. Ellipsometric and FTIR analysis was employed for the optical and chemical analysis. Ellipsometric analysis was found unreliable due to high instrument error relative to the small changes in the intensity. However, for methane exposed to COOH the difference in the relative intensity reflected before and after exposure is large and warrants more investigation. To evaluate this response further, experiments can be done by changing the pressure, concentration and the temperature of the substrate. FTIR analysis further supports the indication that the C-18 monolayer is not a good receptor of methane and propane under the experimental conditions used. However, considerable changes were observed in the COOH chain length after exposure, but their was no clear indication of methane or propane adsorption on the COOH monolayer.

Adsorption of the gas on thin films is also influenced by surface dynamics [12] among other factors. However, because of laboratory constraints the experiment was not designed for in-situ measurements and realtime variation of temperature. Future investigation can be carried out by designing an experiment incorporating in-situ measurements with temperature changes. Furthermore, there is a need to investigate other self assembled monolayers. Gas exposure experiments can also be carried out by mixing the already available monolayers in different proportions to synthesize new monolayers with different surface properties and morphologies suitable for different gases. It would also be interesting to observe the behavior of the NO_x gases to different self assembled monolayers. Keeping in mind the hazards associated with these gases, a dedicated laboratory space would be necessary to carry out real time, in-situ experiments. Atomic force microscopy can also be used to observe changes in the morphology of the SAM after exposure to the gases.

5.2 Spectroscopic Ellipsometry for Characterization and Concentration Measurement of Proteins Immobilized on SAM's.

In this experimental study my emphasis was to shown that it is possible to characterize proteins and measure the concentration of biological samples by measuring the light intensity reflected from thin solid residuals left on a monolayer using spectroscopic ellipsometry. Experiments were done in the visible and NIR region of the electromagnetic spectrum. It was found that the difference in the measured reflected intensity is most sensitive to the protein samples at 0.42 μm wavelength in the visible

region. However, in the case of the NIR region two curves clearly separating the proteins were obtained. The curves looked similar with only difference being in the amount of intensity reflected from the surface, however their is no specific wavelength region distinguishing two proteins. For concentration measurements it was found that the reflected intensity changes were more representative of the change in concentration on a C-18 surface than to COOH. It was also observed that $\tan\Psi$ is a better representative of concentration change as compared to intensity. From FTIR results, it was concluded that the COOH surface is a better choice in terms of reversibility than C-18. It can be presumed from these results that the C-18 is a good surface for concentration measurement and COOH is a better choice in terms of reusability consideration.

For future direction research can be carried out by applying the concept of protein characterization for the early detection of certain types of cancer at a cellular level and genetic diseases which occur due to mutation in the genes. By designing a suitable experiment it is possible to obtain the optical signatures of the rogue proteins and detect the disease in its infancy. Moreover, there is a need to further investigate other self assembled monolayers with surface energies between that of C-18 and COOH, for their suitability toward biological detection. Investigation into this can also lead to the optimization of surface properties which are imperative for reusable and consistent detection. Also experiments can be carried out to identify different functional groups which can act as antibodies for specific analyte capture.

Bibliography

[1] Frank Schreiber. *Progress in surface Sciences*, 65:151–256, 2000.

[2] A. Ulman. *Chem. Rev.*, 96:1533–1544, 1996.

[3] Paul E. laibinis, Bentley J. Palmer, Seok-Won Lee, and G. Kane Jennings. *Thin Films*, 24:1079–4050, 1998.

[4] Technical Bulletin of, Dojindo Molecular technologies, Inc.

[5] P.S Vukusic, G.P. bryan Brown, and J.R Sambler. *Sensors and Actuators B*, 8:155–159, 1992.

[6] T. Nomura, A. Saitoh, and S. Furukawa. *IEEE Ultrasonics Symposium*, pages 525–528, 1998.

[7] R.E. Cavicchi, S Semanchik, R.M Walton, B. Panchapakesan, D.L. DeVoe, and M. Aquinoclass. Part of spie conference boston massachusetts. volume 3857, 1999.

[8] B. Kuswandi, R. Andres, and R Narayanaswamy. *Analyst*, 126:1469, 2001.

[9] *Physical Chemistry of Surfaces.* John-Wiley and Sons, New York.

[10] W. Steele. *Chem Review*, 93:2355, 1990.

[11] I. Langmuir. *J. Am. Chem. Soc*, 40:1361, 1918.

[12] Samuel Glasstone, Keith J. Laidler, and Henry Eyring. *The Theory of Rate Processes.* McGRAW- HILL BOOK COMPANY, INC., 1941.

[13] L.S Miller, A.M McRoberts, D.J. Walton, I.R. Peterson, D.A. Parry, and C.G.D. Sykesud. *Thin Solid Films*, 284-285:927–931, 1996.

[14] L.S. Miller, A.M. McRoberts, D.J. Walton, D.A. Parry, and A.L. Newton. Optical gas sensing using langmuir-blodgett films. *Materials Science and Engineering C*, C3, 1995.

[15] A. Newton, L.S Miller, and I.R Peterson. In A.T. Augousti, editor, *Sensors and their Application*, volume 28. IOP Bristol, 1995.

[16] J. Scheerder, D.J Walton, and I.R. Peterson. *Adv. Mater. Opt. Electron*, 8:309, 1998.

[17] L.S Miller, A.L. Newton, C.G.D Sykesud, and D.J. Walton. *Sensors Technology and Applications*, 139, 1991.

[18] A. Bradford, P.L Drake, O. Worsfold, I.R Peterson, D.J Walton, and G.J. Price. *Phys Chem. Chem. Phys*, 3:1750, 2001.

[19] Hari Singh Nalwa, editor. *Baraton, Handbook of nanostructured Materials and Nanotechnology.* Number 90-153. Academic Press, San Deigo, 2000.

[20] A.W Adamson and A.P. Gast. *Physical Chemistry of Surfaces.* John-Wiley and Sons, New York, 1997.

[21] M. Wulf, K. Grundke, D.Y Kwok, and A.W. Neumann. *J. App. Poly. Sci,* 77:2493, 2000.

[22] M. Zharnikov, S. Frey, H. Rong, Y.J. Yang, K. Heister, M. BUck, and M. Grunze. *Phys. Chem and Chem. Phys.*, 2:3359, 2000.

[23] M. Zharnikov, S. Frey, V. Stadler, W. Eck, K. Heister, and M. Grunze. *Langmuir,* 17:2508, 2001.

[24] F.P. Zamborini and R. M. Crooks. *Langmuir*, 14:3279, 1998.

[25] D.W. Lubbers and N. Opitz. *Zeitschrift Fur Naturforschung*, 30:532–533, 1975.

[26] *Fibre Optic Chemical Sensors and Biosensors*, volume II, pages 193–216. CRC Press, Boca Raton, FL, 1991.

[27] A. Brecht and G. Gauglitz. Optical probes and transduers. *Biosesnors Bio-Electron*, 10:923–936, 1995.

[28] H.C Yang, D.L. Dermondy, C. Xu, A.J. Ricco, and R.M. Crooks. *Langmuir,* page 726, 1995.

[29] M. Wells, D. L. dermondy, H. C. Yang, T. KIm, and R. M. Crooks. *Langmuir,* 12:1989, 1995.

[30] R. Aveyard, B. D. Beake, and J. H. Clint. *Phys. Chem. Chem. Phys.*, 1:2513, 1999.

[31] D. S. Karpovich and G.J. Blanchard. *Langmuir*, 13:4031, 1997.

[32] F. L. Dickert, P. Achatz, W. E. Bulst, W. Greibl, O. Hayden, L. Ping, R. Skorski, and U. Wolff. *SPIE Conference on Chemical Microsensors and Applications II, Boston, Massachusetts*, 116, 1999.

[33] L.H. Dubois and R.G. Nuzzo. *Annu. Rev. Phys. Chem*, 43:437–463, 1992.

[34] A. Ulman. *Chem. Rev*, 96:1533–1554, 1996.

[35] A.R Bishop and R.G. Nuzzo. *Curr. Opin. Colloid Interface Sci*, 1:127–136, 1996.

[36] M. Mrksich and G.M. Whitesides. *Ann. Rev. Biophys. Biomol. Struct.*, 25:55–78, 1996.

[37] C. Roberts, C.S. Chen, M. Mrksich, V. Martichonok, D.E. Ingber, and G.M Whitesides. *J. Am. Chem. Soc.*, 120:6548–6555, 1998.

[38] M. Mrksich, J.R. Grunwell, and G.M Whitesides. *J. Am. Chem. Soc.*, 117:12009–12010, 1995.

[39] Amanda J. Haes. and Richard P. Van Duyne. Mat.res.soc.symp.proc. volume 723, 2002.

[40] Sackmann E. *Science*, 271:43–48, 1996.

[41] P. Schuck. *Annu. Rev. Biophys. Biomol. Struct*, 26:541–566, 1997.

[42] W. Knoll, M. Liley, D. Piscevic, J. Spinke, and M.J Tarlov. *Adv Biophys*, 34:231–251, 1997.

[43] C.A Mirkin and M.A Ratner. *Annu. Rev. Phys. Chem.*, 43:719–754, 1992.

[44] M.A. Rampi, O.J.A. Schueller, and G.M. Whitesides. *Phys. Lett.*, 72:1781–1783, 1998.

[45] D.L Klein, R. Roth, A.K.L Lim, A.P Alivisatos, and P.L Mceuen. *Nature*, 389:699–701, 1997.

[46] L.A Bumm, J.J Arnold, M.T Cygan, T.D Dunbar, T.P Burgin, L. Jones, II; D.L Allara, and J.M. Weiss. *Science*, 271:1705–1707, 1996.

[47] R.D. Piner, J. Zhu, F. Xu, S. Hong, and C.A. Mirkin. *Science*, 283:661–663, 1999.

[48] A. Kumar, H.A. Biebuyck, N.L. Abbott, and G.M. Whitesides. *J. Am. Chem. Soc.*, 114:9188–9189, 1992.

[49] M. Mrksich, G.M Whitesides, R.M. Stroud, W.L. Hubbell, W.K Olson, and M.P. Sheetz. Using self assembled monolayers to understand the interactions of man made surfaces with proteins and cells. *Eds. Annual. Reviews. Inc. Palo Alto, CA.*, 25:55–78, 1996.

[50] Thomas E. Creighton. *Proteins Structures and Molecular Properties.* W. H. Freeman and Co, 1993.

[51] http://www.ornl.gov/.

[52] W.J.H. Van Berkel, R.H.H van den Heuvel, C. Versluis, and A.J.R. Heck. Detection of intact megadalton protein assemblies of vaillyl-alcohol oxidase by mass spectrometry. *Protein Science*, 9:435–439, 2000.

[53] Sprangers R., Groves M.R., Sinning I., and Sattler M. *J. Mol. Biol.*, 21:507–20, 2003. protein structure-NMR,Sattlergroup.

[54] Gale. Rhodes. *Crystallography Made Crystal Clear.* Academic Press, San Diego, 1993.

[55] Carter, Charles W. Jr., and Robert M. Sweet. *eds. Methods in Enzymology*, 276, 1997.

[56] A. Ulman. *An Introduction to Ultrathin Organic Films.* Academic Press: Boston, 1991.

[57] Bigelow. W.C, D.L Pickett, and W.A Zisman. *J. Colloid. Interface.*, 1:513, 1946.

[58] R.G Nuzzo and D.L Allara. *J. Am. Chem. Soc*, 105:4481, 1983.

[59] G.L gaines Jr. *Insoluble Monolayers at liquid-Gas Interfaces.* Interscience and Newyork, 1966.

[60] A. Ulman. *An Introduction to Ultrathin Organic Films: From Langmuir-Blogett to Self-Assembly.* Academic Press, Boston, 1991.

[61] H. Kuhn and A. Ulman. *In Thin Films*, volume 20. Academic Press: New York, 1995.

[62] A. Ulman, S.D Evans, Y. Shnidman, R. Sharma, J.E Eilers, and J.C Chang. *J. Am. Chem. Soc.*, 113:1499, 1991.

[63] Nuzzo R. G., Fusco F. A., and Allara D.L. *J. Am. Chem. Soc.*, 109:2358–2368, 1987.

[64] Folkers J.P, Paul E. Laibinis, and G.M. Whitesides. *Langmuir*, 8:1330–1341, 1992.

[65] Paul E. Laibinis, George M. Whitesides, David L. Allara, Yu-Tai tao, atul N. Parikh, and Ralph G. Nuzzo. *Amer. Chem. Soc.*, 113:7152–7167, 1991.

[66] M.C. Petty. Gas sensing using thin organic films. *Biosens. Bioelectron*, 10:129–134, 1995.

[67] T.Nomura, M.Takeyabayashi, and S.Furukawa. Chemical sensor based on surface acoustic wave resonance incarporating langmuir-blodgett films. pages 445–555. IEEE, Proc. IEEE Ultrason. Symp., 1995.

[68] R. Teppner, S. Bae, K. Haage, and H. Motschmann. *Langmuir*, 15:7002–7007, 1999.

[69] James N. Hilfiker, Corey L. Bungay, ron A. Synowicki, Thomas E. Tiwald, Craig M. Herzinger, Blaine Johns, Greg K. Pribil, and John A. Woollam. *J. Vac. Sci. Technol.*, 21:1103–1108, 2003.

[70] Curtis W. Meuse. Infrared spectroscopic ellipsometry of self-assembled monolayers. *Langmuir*, 16:9483–9487, 2000.

[71] Sopra website. www.sopra-sa.com. Internet.

[72] K. Isaacson, Dr. Daniel Kwok, and Dr. Richard Sun. Spectroscopic ellipsometry measurement of n-alkanethiol self-assembled monolayer thickness. *Under Preparation*, 2004.

[73] J. Yang, J. Han, K. Issacson, and D.Y. Kwok. *Langmuir*, 19:9231, 2003.

[74] P.E. Laibinis G.M. Whitesides, D.L. Allara, Y.T. Tao, A.N. Parikh, and R.G. Nuzzo. *J. Am. Chem. Soc.*, 113:7152, 1991.

[75] A. Ulman. *Chem Rev*, 96:1533, 1996.

[76] G. Kane Jennings and Paul E. Laibinis. *J. Am. Chem. Soc*, 119:5208, 1997.

[77] Laura M. Quattrocci and George E. Ewing. *J. Chem. Phys.*, 96:4205–4215, 1992.

[78] *Affinity Biosensors Techniques and Protocols*. Humanae Press. New Jersey, 1998.

[79] J.Homola, S.S. Yee, , and G. Gaugilz. *Sensors Actuators*, 54:3–15, 1999.

[80] B. Drevillion. *Prog. Cryst. growth Charact.* 27:1–87, 1993.

[81] Azzam R.M. and Bashara N.M. *Ellipsometry and Polarized Light*. North Holland Publication: Amsterdam, 1979.

[82] J.J Ramsden and Q. Rev. *Biophys*, 27:41–105, 1993.

[83] Enric Garcia-Caurel, Bernard drevillion, Antonello De Martino, and Laurent Scwartz. *Applied Optics*, 41(34):7339–7345, 12 2002.